TERRESTRIAL EFFECTS OF HIGH ENERGY COSMIC RAYS

BY

Dimitra Atri

Submitted to the graduate degree program in Physics and the Graduate Faculty of the University of Kansas in partial fulfillment of the requirements for the degree of Doctor of Philosophy

Chair: Prof. Adrian L. Melott

Prof. Carey K. Johnson

Prof. Michael J. Murray

Prof. Brian C. Thomas

Prof. Graham W. Wilson

Date defended: April 5, 2011

The Dissertation Committee of Dimitra Atri certifies

that this is the approved Version of the following thesis:

TERRESTRIAL EFFECTS OF HIGH ENERGY COSMIC RAYS

Chair: Prof. Adrian L. Melott

ABSTRACT

On geological timescales, the Earth is likely to be exposed to higher than the usual flux of high energy cosmic rays (HECRs) from astrophysical sources such as nearby supernovae, gamma ray bursts or by galactic shocks. These high-energy particles strike the Earth's atmosphere, initiating an extensive air shower. As the air shower propagates deeper, it ionizes the atmosphere by producing charged secondary particles and photons. Increased ionization leads to changes in atmospheric chemistry, resulting in ozone depletion. This increases the flux of solar UVB radiation at the surface, which is potentially harmful to living organisms. Increased ionization affects the global electrical circuit, which could enhance the low-altitude cloud formation rate. Secondary particles such as muons and thermal neutrons produced as a result of hadronic interactions of the primary cosmic rays with the atmosphere are able to reach the ground, enhancing the biological radiation dose. The muon flux dominates the radiation dose from cosmic rays causing damage to DNA and an increase in mutation rates and cancer, which can have serious biological implications for surface and sub-surface life. Using CORSIKA, we perform massive computer simulations and construct lookup tables for 10 GeV - 1 PeV primaries, which can be used to quantify these effects from enhanced cosmic ray exposure to any astrophysical source. These tables are freely available to the community

and can be used for other studies. We use these tables to study the terrestrial implications of galactic shock generated by the infall of our galaxy toward the Virgo cluster. Increased radiation dose from muons could be a possible mechanism explaining the observed periodicity in biodiversity in paleobiology databases.

Contents

List of Tables

List of Figures

Chapter 1

Introduction

1.1 Planetary life in the astrophysical radiation environment

We are a part of an ever evolving and dynamic Universe. Ever since the big bang, matter has evolved and been shaped into a variety of forms including a form with the capacity to think. As far as we know, the Universe is 13.7 billion years old and Earth formed much later, 4.5 billion years ago. The suitable conditions for life to survive and thrive on our planet have existed for 3.5 - 4 billion years. It has only been possible under these unique set of physical conditions that molecules are able to replicate and transfer genetic information. These conditions are governed by the properties of our host planet, star and

our location in the planetary system and Galaxy at a particular time. The astrophysical radiation environment shapes our natural habitat and events occurring in our stellar and galactic neighborhood are most likely to affect the life on our planet. Put aptly by Carl Sagan, "The evolution of life is driven in parts through mutations by the deaths of distant stars...we are, in a very deep sense tied to the cosmos."

Astrophysical radiation consists of both photons and protons from the host star as well as particles of galactic and extragalactic origins, known for historical reasons as cosmic rays. Both particles and photons interact with the planetary atmosphere in different ways. Since we get a high flux of radiation in the form of photons from the host star, considerable effort has been made in order to understand its interaction with the atmosphere and its subsequent effects on our environment and the biosphere. The flux from particles is relatively small and of low energy and does not have a profound effect in our daily life. However, on long timescales, the flux of this radiation could have been much higher on several occasions and would have affected the biosphere [81].

1.2 Cosmic Rays

Cosmic Rays are generated by charged particle acceleration in high-energy astrophysical processes. The flux of particles impinging on the Earth's at-

mosphere can be represented by broken power laws with three regions with different slopes indicating different types of astrophysical sources generating them. The flux of incoming particles consists of about 90% protons, about 9% alpha particles and the rest are heavy nuclei [29,83]. Although these numbers differ slightly from experiment to experiment, this composition is widely accepted for normal energies. The composition changes considerably at very high and ultrahigh energies [16, 45, 108]. Depending on their origin, these particles, or cosmic rays can be classified into solar cosmic rays (SCRs), galactic cosmic rays (GCRs) and extragalactic cosmic rays (ECRs).

The term"cosmic rays" in the literature usually refers to galactic cosmic rays (GCRs). GCRs are generated by supernovae shocks within our galaxy and are capable of accelerating particles up to PeV energies. Most particles arriving on the Earth from galactic sources lie in the 1 - 10 GeV range and the spectrum falls sharply above this energy range. Particles accelerated from the Sun reach a maximum of MeV energies and produce ionization at very high altitudes. Although recent observations of enhanced muon flux during solar flares suggest GeV range protons hitting the Earth's atmosphere, it is not clear whether such protons are accelerated by the Sun or within our atmosphere. Ultrahigh energy cosmic rays (UHECRs) (10^{15} eV - 10^{18} eV) are thought to be produced from sources outside our galaxy from Active Galactic Nuclei

(AGNs) [12], Gamma Ray Bursts [24, 27, 85] or from past galactic GRBs [26]. The probability of UHE particles hitting the atmosphere is very small due to the steep spectrum and there are only a very few particles known to date falling with EeV energies. The composition of primaries at these energies is also not well known. The highest energy cosmic rays observed to date are estimated having 10^{21} eV energy.

1.3 Cosmic Ray variations

Cosmic ray variations associated with the solar cycle with a 11-year period are well studied. They are anti-correlated with the solar activity and primaries less than about 10 GeV energy are modulated by this effect. These low energy primaries strike high up in the atmosphere and have negligible impact when secondary particles arrive at the ground level. The normal CR flux is dominated by low energy primaries (Figure 1.1) that are easily deflected by the geomagnetic field. As a result, one detects a higher flux of CRs toward the poles than the equator. Primaries up to about 17 GeV are guided by the geomagnetic field. The CR flux increases with altitude and the resulting mutagenic effects have been often discussed in the context of air [15,39] and space travel [22,123]. Since the flux of the high energy component of the normal CR spectrum is very low, its effects on our daily lives are negligible and therefore

have not been studied in the context of their atmospheric and biological effects. Erlykin and Wolfendale [36] also discuss long term cosmic ray variations and their biological effects from a number of astrophysical sources. On geological timescales, the Earth is likely to be exposed to an increased flux of high energy cosmic rays (HECRs) from astrophysical sources such as nearby supernovae, gamma ray bursts or by galactic shocks. These high-energy particles strike the Earth's atmosphere initiating an extensive air shower of particles that can reach the ground and cause damage.

Supernovae are believed to be the source of galactic cosmic rays (GCRs), capable of accelerating the particles up to 10^{15} eV. Sources of ultra-high energy cosmic rays (UHECRs) are not well established but GRBs and AGNs are the primary candidates potentially capable of accelerating particles up to 10^{19} eV. There are cosmic ray flux variations associated with geomagnetic field reversals but they have been found to have limited impact on our planet [43].

On the other hand, the primary source of low energy protons is the Sun, responsible for MeV range primaries directed toward the poles because of the geomagnetic field.

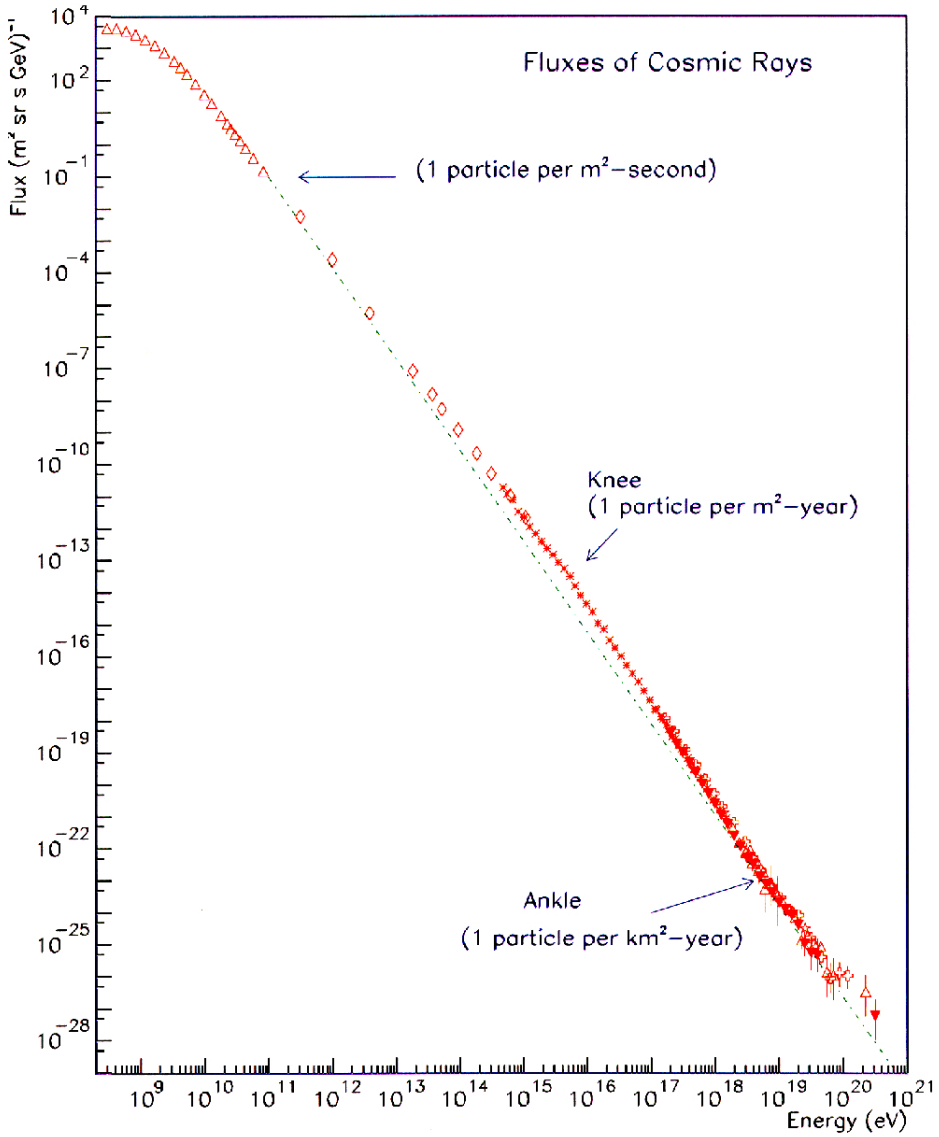

Figure 1.1: Cosmic Ray Spectrum can be described by a broken power law. Vertical axis is the differential flux and the horizontal axis is the kinetic energy of the incident primaries ranging from 0.1 GeV to 1 ZeV [110]

1.4 Radiation and terrestrial effects

From an astrobiology perspective, there are two primary mechanisms of high-energy astrophysical radiation causing damage to the biosphere. One is the well studied damage from enhanced UVB (280 - 315 nm) flux at the ground resulting from ozone depletion by high-energy radiation. Both cosmic rays and photons can ionize the atmosphere and the resulting photochemical changes deplete ozone in the upper stratosphere. Another mechanism is the direct irradiation of secondary particles produced in the atmosphere (primarily muons and thermal neutrons), on living organisms. An intense photon burst can ionize the upper atmosphere and result in significant changes in atmospheric chemistry from photochemical reactions. The ozone layer in the upper stratosphere is depleted due to this ionization and converted to oxygen. Ozone blocks the harmful UVB radiation from the Sun, and the flux of UVB increases on the ground due to this depletion. UVB radiation is known to be carcinogenic and can cause DNA damage and result in a number of diseases.

The low energy particles of solar origin strike the Earth's upper atmosphere. Secondary particles produced as a result are absorbed high up in the atmosphere. The level of damage to the upper atmosphere is very limited. More energetic particles known as galactic cosmic rays strike the atmosphere. A low dose of secondary particles reaches the earth's surface and is known to

have harmful effects on terrestrial life [63, 64]. There have been some studies of climatic changes from the 11 year solar cycle associated with GCRs which will be discussed later [34, 54, 55, 109]. Higher energy primaries can strike the earth on long timescales. This higher energy component of the CR flux would increase significantly in case of extreme events such as GRBs [112, 115], nearby supernovae [33, 41, 47, 113] and solar dynamics within the galaxy [77], and could significantly affect the environment and life on our planet. There have been suggestions postulating a threat to life on Earth due to energetic phenomena generating cosmic rays. Dar et al. [23] proposed the idea that cosmic ray bursts from mergers of neutron stars could cause a mass extinction on Earth. Shaviv et al. [104] proposed the idea of global cooling due to CRs. Normal cosmic ray variations have been found to be correlated with cancer rates [63, 64].

Cosmic rays can deplete the ozone layer and enhance the global cloud cover; a muon burst on the ground could directly affect living organisms. These effects form normal cosmic radiation are too small to have any serious impact on our normal life and not much attention has been paid. But these effects become important in case of impact from extreme astrophysical events that are relevant on long timescales.

There have been studies involving detailed computational modeling of the

atmospheric effects of GRBs and nearby supernovae, and the subsequent effects on life have been evaluated using only photons [32, 103, 112]. Most photons are much lower in energy than galactic cosmic rays and are unable to initiate an air shower. However, GeV photons generated by short-hard bursts (SHBs) can produce air showers and can produce results similar to those of cosmic rays. Photons ionize the upper atmosphere depleting the ozone layer allowing exposure to more UVB radiation from the Sun.

There has been no quantitative analysis of the terrestrial effects of high energy cosmic rays so far. As opposed to the lower energy CRs, the high energy CRs ($> 17GeV$) are not affected by the geomagnetic field and one would observe a uniform flux throughout the globe. Also, they penetrate much deeper into the atmosphere, enhancing atmospheric ionization closer to the ground than normal. The harmful secondary muon flux on the ground would be of much higher energy, capable of penetrating deep under rock and water. Only approximate analytical estimates of the biological effects from enhanced CRs have been made [46].

This work is an attempt to quantify these effects by detailed computational modeling of the atmospheric propagation of cosmic rays and exploring the resulting atmospheric and biological impact.

1.5 Dissertation outline

In chapter 2, I will summarize the physics of the atmospheric interaction of cosmic rays and the Monte Carlo tool CORSIKA used for modeling. Chapters 3 and 4 detail the modeling of these interactions and construction of lookup tables that can be used by researchers for various studies. We then use these tables to compute various terrestrial effects from the extragalactic shock and discuss their implications on the Earth's atmosphere and life in Chapter 5. Other potential applications and further work is discussed in Chapter 6, followed by a discussion in Chapter 7.

Chapter 2

Air showers and CORSIKA

The density of intergalactic and interstellar space is very small and particles can travel almost unhindered in space, guided by the magnetic fields, until they encounter an abrupt increase in density, the planetary atmosphere.

2.1 Air showers

Primary cosmic ray protons or other nuclei enter the atmosphere and strike the nuclei of nitrogen or oxygen and produce secondary particles as a result of this inelastic collision. These high energy protons are subjected to the strong interaction when they collide with the nuclei of N_2 and O_2 molecules, producing secondary particles and photons. The majority of the secondary particles produced consist of pions.

The primary proton's interaction with protons in the atmosphere is given by:

$$p + p \rightarrow p + n + \pi^+$$

$$p + p \rightarrow p + p + \pi^0$$

And the primary proton's interaction with neutrons in the atmosphere is given by:

$$p + n \rightarrow p + p + \pi^-$$

$$p + n \rightarrow p + n + \pi^0$$

$$p + n \rightarrow n + n + \pi^+$$

It must be noted that particle multiplicities increase with increasing energies and the number of particles produced in these interactions change accordingly. Other particles such as baryon-antibaryon pairs and kaons are also produced at high primary energies. These secondary particles either decay to produce other particles or interact with other particles in the atmosphere. Such a cascade of particles is known as a hadronic shower. Neutral pions produced at the first interaction decay into photons which initiates a cascade of secondary electrons, positrons and photons, called the electromagnetic shower.

$$\pi^0 \rightarrow \gamma + \gamma$$

The muonic component is fed by the lower energy charged kaons and pions. This combined cascade of particles and photons grows as it propagates in the atmosphere and is called an Extensive Air Shower (EAS). Air showers from high-energy cosmic rays can spread over a few tens of square km area, depending on their energy. They are detected by ground based detectors or by telescopes looking for Cherenkov radiation from the air shower. This description of CR-induced air showers is primarily derived from these books: [29, 44, 99, 107].

These secondary particles further collide with other nuclei, starting a chain of reactions known as the hard and nucleonic components of the CR shower (Figure 1.2). All particles produced suffer energy loss through electromagnetic and/or hadronic interactions in the atmosphere. The primary will either collide with a proton or a neutron of the N_2 or O_2 nucleus producing pions.

Charged pions have a mean half life of 26 ns and they may further undergo collisions before decaying. Neutral pions on the other hand have a half life of 10^{-16} s and decay into gamma rays (without undergoing collisions due to their short half life), which produce electron positron pairs and undergo bremsstrahlung subsequently producing electron positron pairs (as long as the photon energy exceeds 1.02 MeV), building up the electromagnetic component of the shower.

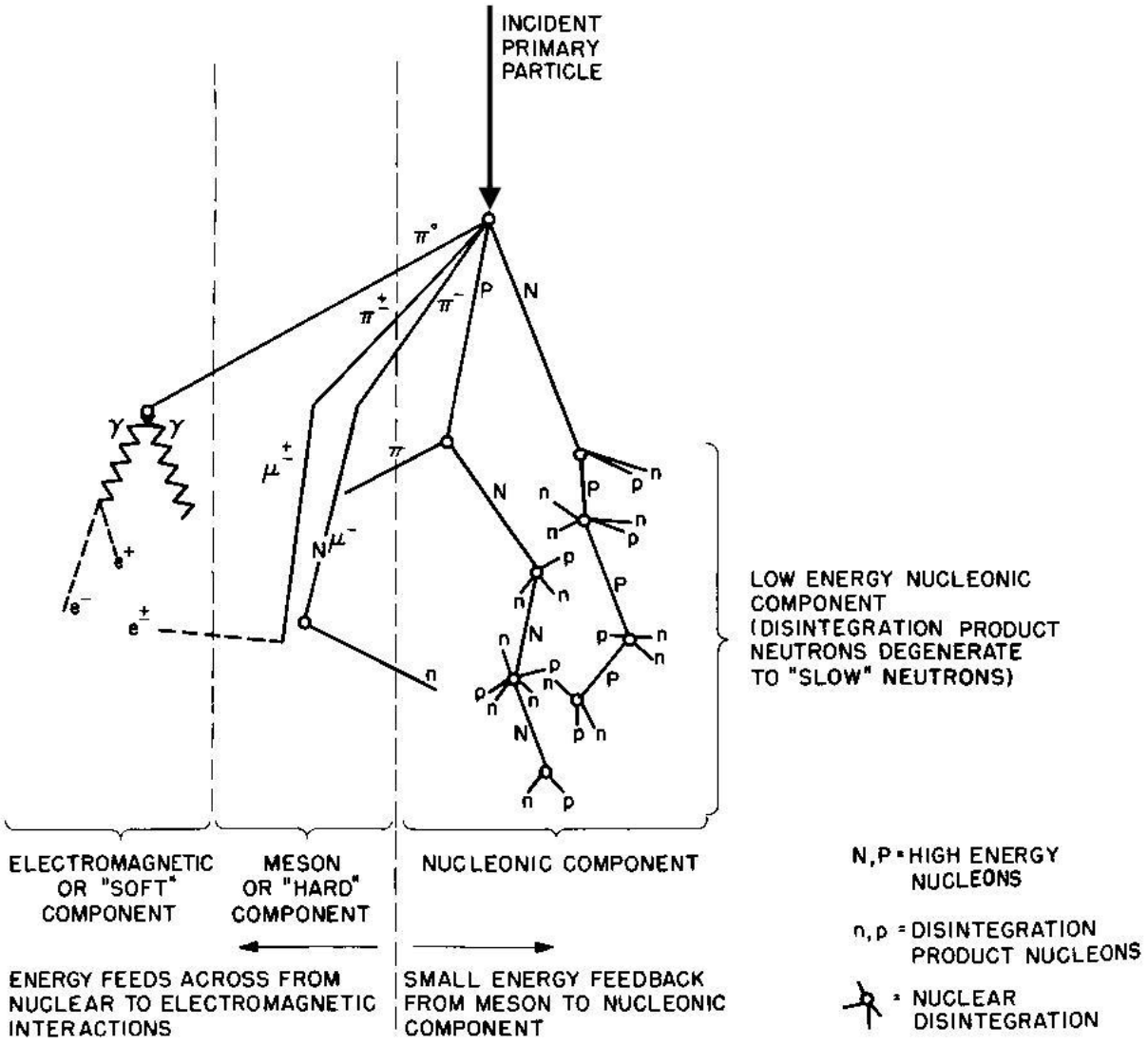

Figure 2.1: Air shower (Credit: DESY)

2.1.1 Electromagnetic cascade

The electromagnetic cascade is a combination of the interactions of photons and electrons with the atmospheric nuclei. Both photons and electrons interact with matter in different ways. The photon interaction can be described by pair production, photoelectric effect and the Compton effect. Pair production is the dominant process at energies $> 100\ MeV$ where the photon interacts with the Coulomb field of the nucleus resulting in the production of an electron-positron pair. The photon kicks off an electron from an atom in the photoelectric effect. It is relevant only at very low energies since the photoelectric cross section is very small at higher energies. Photons can also interact with free electrons where they can transfer energy upon interaction, also known as the Compton effect. This effect is also relevant at the MeV energy level.

The interaction of electrons with matter is through ionization and bremsstrahlung. Ionization can be calculated by the following equation:

$$\frac{dE}{dx} = 2m_e[ln(\frac{\pi^2 {m^2}_e}{(1-\beta^2)^{3/2} I^2(Z)}) - a] \tag{2.1}$$

Where $\frac{dE}{dx}$ is in units of $eVg^{-1}cm^2$, $I(Z)$ is the average ionization potential (in eV) of an atom in the medium Z, x is the column density in gcm^{-2}, $\beta = \frac{v}{c}$, a is a constant which is 2.9 for electrons and 3.6 for positrons. The other

process is bremsstrahlung where a photon is emitted after the interaction of an electron with the electromagnetic field of the nucleus.

2.1.2 Hadronic component

The hadronic component consists of cascades generated by hadronic interactions of nuclei as described earlier. Particle flux of type j at a given atmospheric depth X is given by [44]:

$$\frac{dF_j(E,X)}{dX} = -(\frac{1}{\lambda_j} + \frac{1}{d_j})F_j(E,X) + \sum_i \int \frac{g_{ij}(E_i,E_j)}{dE_i}\frac{F_i(E_i)}{\lambda_i}dE_i \qquad (2.2)$$

Where λ_j is the mean free path for inelastic interactions of particle j, decay length is d_j and σ_j is the cross section. The second term in the above equation is the source term that sums over the secondary particle j production with energy E_j by primary particles of type i with energy E_i. The term $\frac{g_{ij}(E_i,E_j)}{dE_i}$ is the spectrum of secondaries from the decay of particles and $\frac{F_i(E_i)}{\lambda_i}dE_i$ is the spectrum of the decaying parent particles.

Mean free path for inelastic interactions, λ_j is given by:

$$\lambda_j = \frac{A}{N_A\sigma_j} \qquad (2.3)$$

Where A is the mean atomic mass of the medium, and σ_j is the cross section.

2.1.3 Muon component

Muons are produced primarily from the following decay processes:

$$\pi^+ \rightarrow \mu^+ + \nu_\mu$$

$$\pi^- \rightarrow \mu^- + \bar{\nu_\mu}$$

They have a mass of 105.7 MeV/c^2, which is around 200 times the mass of an electron and a lifetime of 2.2 μs. They decay into secondary particles as follows:

$$\mu^- \rightarrow e^- + \nu_e + \nu_\mu$$

$$\mu^+ \rightarrow e^+ + \nu_e + \nu_\mu$$

However, because of the relativistic γ factor, most muons are able to reach the ground without decay, especially at higher primary energies.

The main process by which muons lose energy below TeV energies is through ionization as they travel in the atmosphere. Ionization loss is given by the Bethe-Bloch equation:

$$\frac{dE}{dx} = \frac{4\pi}{m_e}.\frac{nz^2}{\beta^2}.\left(\frac{e^2}{4\pi\epsilon_0}\right)^2.[ln(\frac{2m_e c^2\beta^2}{I.(1-\beta^2}) - \beta^2] \tag{2.4}$$

Above TeV energies, losses due to bremsstrahlung and electron-positron pair production are also significant.

2.2 Monte Carlo code: CORSIKA

In order to trace all the interactions and particles produced in the cascade, one needs to (1) solve cascade equations to propagate the electromagnetic part of the shower and (2) solve propagation equations to include nuclear interactions of all the secondary particles produced. This becomes very hard to solve analytically and Monte Carlo tools are used widely to model air showers. The Monte Carlo method is a brute force method that uses randomly generated values for uncertain variables. It is a computationally intensive method since one needs to repeat the process a number of times in order to generate output and average it out. In air shower physics, one uses the method to generate spatial and momentum coordinates of all the particles produced in the interactions and track the shower and sub-showers down to the ground. One must note that as we reach primary energies higher than current accelerator experiments, the nuclear interaction cross sections are not known. Also, the composition of primaries at very high energy is not known precisely. Monte Carlo tools have been used to solve cascade equations for a long time but they lacked the physics of interaction at high energies. CORSIKA was devel-

oped [58] in order to study air showers from primaries much higher in energy than the ones studied in laboratory experiments. The hadronic interaction cross sections used in CORSIKA are theoretical, and one can choose from a variety of hadronic interaction models available. The results from CORSIKA are compared with the experimental data from the KASCADE experiment [3], which allows theorists to fine tune the hadronic interaction cross sections. A number of cosmic ray researchers around the globe now use CORSIKA and contribute to this process. Hence, this model has evolved into a robust and more accurate Monte Carlo tool than initially conceived.

CORSIKA (COsmic Ray SImulations for KAscade) is a Monte Carlo code used extensively to study air showers generated by primaries up to 100 EeV. It is primarily calibrated by KASCADE data, which is a detector used to study hadronic interactions in the 10^{16} to 10^{18} eV energy range. Overall CORSIKA simulations are consistent from 10^{12} eV, the typical range of Cherenkov detectors, up to the highest energies observed 10^{20} eV. The code can propagate primary photons, protons and heavier nuclei up to Fe.

One can choose the following hadronic interaction models for simulations: for high energies VENUS [122], QGSJET [65], DPMJET [98], SIBYLL [42], HDPM [18] and EGS4 [86] (photoproduction of muon pairs and hadrons). A good comparison with experimental data has been done for p, α, O, Fe, γ

primaries in the 10^{11} - 10^{16} eV range. Ionization loss is calculated by the Bethe-Bloch formula. Hadronic interactions at lower energies are described by FLUKA [10, 37], UrQMD [9, 14] and GHEISHA [40] models.

The code includes a number of details of the atmosphere. The elemental composition of the atmosphere is built in and can be changed if needed. It has been set to 78.1% N_2, 21.0% O_2 and 0.9% Ar by volume. Seasonal variation of atmospheric density with height is also included. For inclined showers, the curvature of the atmosphere has also been taken into account. Data on all particles is tracked and recorded up to the cut-off energy specified at the beginning of the simulation. Different cut off energies can be specified for muons, electrons, photons and hadrons, depending on the purpose of the calculation.

2.3 Hadronic interaction models

Here we describe the different hadronic interaction models we have used for this work. These models are constantly updated and compared with experimental data from around the world. All models have their strengths and weaknesses. Some models might be good in reproducing the atmospheric ionization profile but not the muon energy distribution at the surface etc. Therefore, we have used different combinations of models for different purposes. For atmospheric ionization, we have used EPOS and UrQMD whereas for the muon work, EPOS

and FLUKA were used.

2.3.1 EPOS

EPOS [94] is a high-energy hadronic interaction model used in CORSIKA. It is a new theoretical model consistent with experimental data from RHIC and SPS (CERN). We used the EPOS 1.99 version with improved cross sections compared to the EPOS 1.61 model which produced a larger muon flux at the ground level than observed by KASCADE. The proton-air inelastic cross sections are much improved in this model compared to SIBYLL and QGSJET II and are in excellent agreement with air shower experiments [92].

2.3.2 UrQMD

UrQMD [9, 14] or the Ultrarelativistic Quantum Molecular Dynamics model is the low energy hadronic interaction model simulating ion collisions in the lower energy range (up to 200 GeV). UrQMD is much slower to run than FLUKA, but provides a more accurate ionization profile in the atmosphere.

2.3.3 FLUKA

FLUKA [10,37] is a robust Monte Carlo model used to simulate particle transport through matter which is widely used in a number of particle physics stud-

ies. In cosmic ray physics, it has been found to be consistent with muon data from ground based detectors. When implemented with CORSIKA, we also found it to be much faster than UrQMD.

Chapter 3

Modeling high-energy cosmic ray induced atmospheric ionization

3.1 Ionization modeling at lower energies

As described earlier, as the shower progresses toward the ground, it ionizes the atmosphere along the way. The ionization profile in the atmosphere depends both on the incidence angle and the energy of the primary. One can approximately calculate the atmospheric ionization purely based on electromagnetic interactions using coupled cascade equations. This approach ignores any energy loss due to nuclear interaction and therefore can only be applied to the upper atmosphere, above the point of first nuclear interaction, which is usually around 50 km altitude. Ionization is calculated using the Bethe-Bloch equa-

tion, which calculates the energy lost by a charged particle traversing through a medium. In order to accurately account for both the electromagnetic and nuclear cascade, one needs to employ a more complicated technique that can include both electromagnetic and nuclear cascades.

Vitt and Jackman developed an analytical model [120] to calculate ionization profiles. It is a simple model and can be used for low energy primaries to compute the ionization profile in the upper and middle atmosphere. But the main disadvantage of this model is the lack of hadronic interactions. Therefore, it cannot be applied to the lower atmosphere or higher-energy primaries. Usoskin et al. developed a new model [117] to compute atmospheric ionization resulting from GCR variations in the solar cycle. Their primary energy range goes from 100 MeV to 1 TeV, with only 3 data points (30, 100 and 300 GeV) between 10 GeV and 1 TeV. This model was based on CORSIKA simulations and is in excellent agreement with experimental data. It is not possible to evaluate the atmospheric ionization profiles of primaries higher than a TeV using this model. Also, data is binned in 50 $g\ cm^{-2}$ bins which is too large for interpolation to the photochemical model described briefly in the next section. Therefore we needed new calculations to serve both purposes.

3.2 Description of modeling

Modeling was done such that we have high resolution data from primaries covering 5 orders of magnitude in primary energy. It enables us to interpolate data to the photochemical model. Results are made available in the form of lookup tables so that atmospheric ionization can be calculated from the cosmic ray spectrum of any astrophysical source.

The table we have generated gives energy deposition in bins corresponding to those used in the NASA-Goddard two-dimensional atmospheric chemistry code, hereafter NGSFC [20, 30, 60]. The atmosphere is divided in pressure bins, which correspond approximately to 2 km each, as opposed to column density bins in CORSIKA. In the lower atmosphere, the column density is very high and therefore interpolating is not a problem from other models using column density since one can include a number of bins in 2 km. But at higher altitudes, the column density is too small, and one 50 $g\ cm^{-2}$ bin used in the previous study [117] is too large to interpolate. Our primary motivation when computing atmospheric ionization was to study photochemical changes in the upper stratosphere. Directly using Usoskin et al. model would have resulted in large errors. Therefore we use 1 $g\ cm^{-2}$ column density bins in CORSIKA for better interpolation at higher altitudes. This is the smallest bin size available in the code.

The NGSFC code has been used extensively to study the effects of supernovae [47], gamma-ray bursts [114] and solar proton events on the atmosphere [59,111]. We will only briefly describe this code, given detailed accounts elsewhere [59, 61, 114]. There are 58 log pressure bands (we use only the first 46 of these bins here, as discussed below) and 18 bands of latitude. The model computes atmospheric constituents with a largely empirical background of solar radiation variations, with photodissociation, including small scale mixing and winds. Also, it includes an empirical background of CR source ionization based on current levels, which includes an 11-year solar modulation cycle, all with a one day timestep. The code takes ionization energy flux in a 2-dimensional format using altitude and latitude.

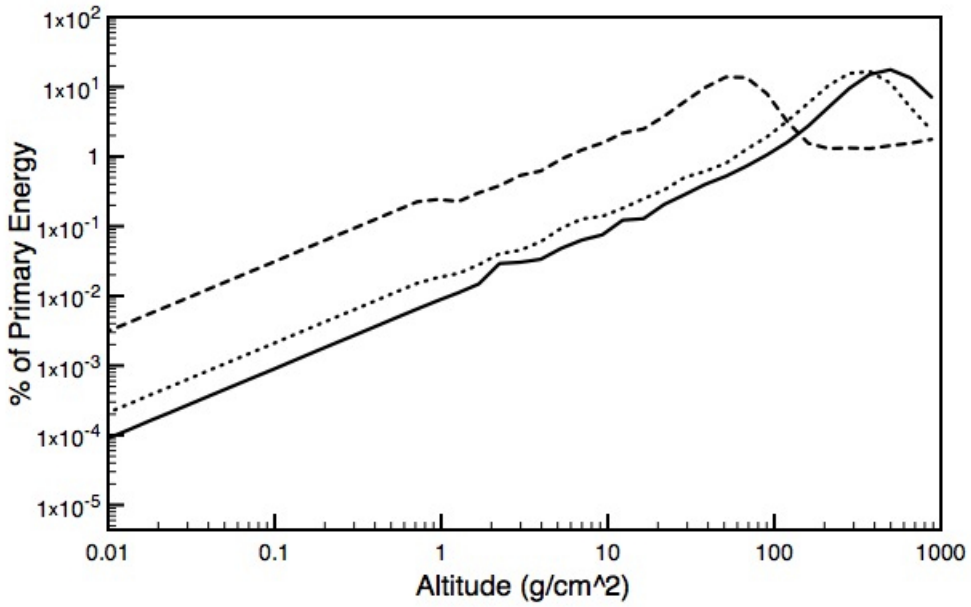

Figure 3.1: Fractional energy deposition for a 10 TeV primary at 5^o (solid), 45^o (dotted), and 85^o(dashed) zenith angles in bins of the NGSFC code in log pressure, which is approximately linear in altitude. The size of each bin is approximately 2 km.

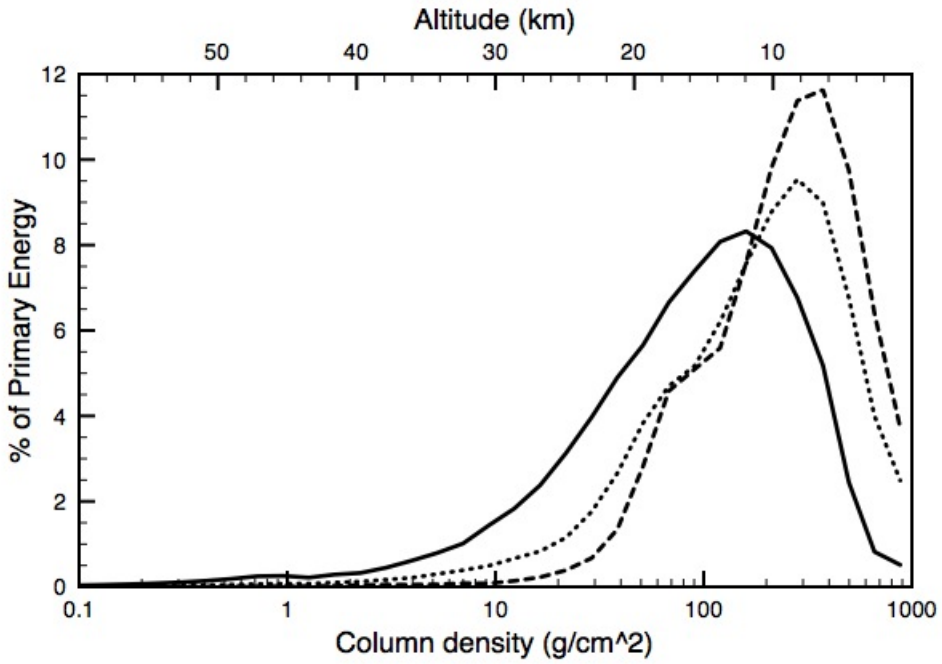

Figure 3.2: Electromagnetic energy deposition from a 100 GeV primary (solid), a 10 TeV primary (dotted) and a PeV primary (dashed) per $g\ cm^{-2}$, in bins of NGSFC code . Energy deposition for the higher energy primaries is deeper in the atmosphere. Energy going into nuclear interactions or hitting the ground is not included in this figure.

CRs of $10^{10} - 10^{15}\ eV$ are of much larger primary energy than those that dominate normal galactic CRs, so one should not simply turn up the usual background, as in a previous supernova study [47]. We used CORSIKA, which is designed to perform detailed simulations of extensive air showers initiated by high energy cosmic ray particles. We did 25 simulated showers at each of a series of energies by 0.1 in $\log_{10}$ intervals of primary energy between 10 GeV

and 1 PeV, i.e. at 51 different primary energies.

We created a lookup table using data from CORSIKA runs that contains atmospheric ionization energy deposition per primary due to CRs in the range of 10 GeV - 1 PeV. The sum of deposition over altitude is less than the total of the primary energy, as not all energy is deposited in the atmosphere by electromagnetic processes. Nuclear interactions also occur between HECRs and atmospheric particles, but nuclear energy is dumped mostly into nuclei, not into atmospheric chemistry. Energy that goes into nuclear interactions or reaches the ground is not included in the deposition table.

An arbitrary spectrum can be convolved with this data and the results used in the NGSFC code (or other similar codes) to simulate the effects this energy flux deposition will have on atmospheric chemistry. It is computationally unfeasible at this time to do Monte Carlos over a very large number of angles of incidence. Because of this, we investigated and applied an approximation scheme. We investigated the effect of zenith angle by running 50 shower ensembles (2500 primary particle simulation runs) at zenith angles of 0^o (vertical), 45^o, and 70^o at 10^{13} eV. In Figure 3.1 we show the fractional energy deposition for each of these zenith angles (excluding nuclear interactions) per bin (bins of the NGSFC code) in log pressure. The size of each bin is approximately 2 km in altitude. Note that the lateral displacement in the lines, and the

location of their maxima, are reasonably approximated by a $(cos\ \theta)^{-1}$ factor, confirming the simplest thing one would expect from a column density factor. For a general-purpose code at the energies we consider, it is appropriate to assume the flux to be isotropic.

For each shower, we recorded the fractional energy deposition in each of 1036 bins of 1 $g\ cm^{-2}$ column density. We used their mean to construct a lookup table describing the energy deposition for a particle of given primary energy as a function of pressure. Below we describe in detail the construction and use of the table.

The greatest deposition of energy per bin corresponds to the first interaction between the incoming CR and the atmosphere, which occurs very high in the atmosphere. Since log column density is nearly linear with altitude, we analyze the maximum energy deposition per bin of log column density. This has weak trends with primary energy, as shown in Figure 3.2. This gives about 100-200 $g\ cm^{-2}$ for 70^o zenith angle as the site of the greatest deposition of energy per unit distance, corresponding to an altitude of about 11-16 km. This can be compared with (a) about 13 km as the mean altitude of maximal energy deposition density for the normal CR spectrum as implemented in the NGSFC code, strongly biased toward latitudes above 60 degrees, and (b) 22 to 35 km as the peak deposition for $keV - MeV$ photons, depending upon en-

ergy [32,114]. One would expect higher energy CRs to penetrate deeper based on their smaller cross sections. This apparent discrepancy between the altitudes in (a) and our CR data results from the fact that the normal dominant CR spectrum up to about a GeV, strongly interacts with the Earth's magnetic field, comes down with a small zenith angle near the poles, and consequently encounters a lower mean column density than an isotropic ensemble.

The table was originally created to compute ozone (O_3) depletion and other atmospheric chemistry changes [79] resulting from energy deposition by HECRs. O_3 concentration in the atmosphere is highest between altitudes of 10-35 km [53] with considerable latitude dependence [32]. Our data is inaccurate by 5% (described later) from 46-90 km because CORSIKA runs on a linear column density scale starting with 1 $g\ cm^{-2}$. However, the main effects of atmospheric chemistry changes on the biosphere occur at lower altitudes. The 46-90 km altitude range is less significant because high-energy CRs rarely have their first interaction that high in the atmosphere.

The CORSIKA model 6.900 is used in all simulations. When installing CORSIKA, UrQMD was used for the low energy hadronic interaction model and EPOS as the high energy hadronic interaction model. CORSIKA was installed with CURVED, SLANT and UPWARD options to simulate primaries at large zenith angles and track upward going particles in a curved atmosphere.

The following are the important variables used in the input file (Table 3.1) for CORSIKA. The Longitudinal Shower Development variable (LONGI) is set as LONGI T 1 T F giving longitudinal ionization for every 1 $g\ cm^{-2}$ bin to facilitate interpolation to the bins of GSFC photochemical code. The variable THETAP gives the angle of incidence of particles and was set as THETAP z z, where z is the zenith angle. The code ran for zenith angles 5^o, 15^o...upto 85^o, a total of 9 angles. The energy range variable (ERANGE) is set as ERANGE x x, where x is the variable energy of the primary particle. For our preliminary runs (10 GeV - 100 TeV), CORSIKA was run 100 times at each of the energies stated above using different SEED random number variables from the input file for each run. The data file outputs a variety of information. The sum of the average longitudinal energy deposited in GeV given at every 1 $g\ cm^{-2}$ is the only data we are interested in order to evaluate the atmospheric ionization. In the future we plan to extend this table above the PeV range.

CORSIKA ran at 51 different energy levels 100 times each at intervals of 0.1 in log energy for 9 angles. Each time it was run CORSIKA simulated 15 protons entering the atmosphere. Therefore, we compiled 13500 particles for each of the 51 energy levels. The energy was averaged for each of the 900 runs at each longitudinal pressure bin.

Minor problems arose when transferring the CORSIKA data to the NGSFC

code. First, the smallest atmospheric depth bin at which energy deposition is given is 1 $g\ cm^{-2}$ in CORSIKA, while 22 of the 46 pressure levels are below 1 $g\ cm^{-2}$ in the NGSFC code. Secondly, CORSIKA outputs deposition in a linear pressure scale. We interpolated to a logarithmic scale for the NGSFC code. We converted CORSIKA atmospheric depth units of $g\ cm^{-2}$ to millibars (needed for NGSFC) by a conversion factor of 0.98.

To resolve the problem of CORSIKA's highest interaction altitude being below 22 of the NGSFC codes altitudes we linearly extrapolated the data using the ionization from the 1 $g\ cm^{-2}$ bin. Because the first interaction point of primaries is rarely within the first $g\ cm^{-2}$, most of the CORSIKA output files have no energy deposition for this altitude. Also, the data we used from CORSIKA is binned in 0.1 GeV intervals, meaning for the lower energy runs many of the 1036 altitude levels are zero. For this reason our output file may have no energy in the 22 highest altitude bins for certain energy levels. For our purpose of looking at the ozone these higher altitudes, above $\sim$ 46 km, are not important, since the amount of ionization in them from HECR would be quite small.

We use the same linear interpolation method for each bin with less than 1 $g\ cm^{-2}$, depositing the energy from ground level to the highest logarithmic altitude level in the last bin, as shown in table 3.3. The logarithmic altitude

bins are centered on the bins used in the NGSFC code (Table 3.2).

The geomagnetic field should be mentioned with regard to the lookup table. Its impact on CRs is minor for protons with energies greater than 17 GeV. Because this only impacts a small region of the CR range of importance (10 GeV - 1 EeV) effects due to the magnetic field are small. If desired, alterations to the latitude distribution of energy deposition can be made in the 10 to 17 GeV range to simulate the effects of deflection by the geomagnetic field.

We present results in the form of two lookup tables that give (1) atmospheric ionization corresponding to column density and (2) atmospheric ionization corresponding to the bins of NGSFC code. The lookup tables are formatted into 51 columns corresponding to 51 energies but the number of rows for both tables are different. For the atmospheric chemistry model, the table has 46 rows corresponding to the altitude bins of the NGSFC code shown in table 3.2. As is, it displays ionization energy deposition for a spectrum of 1 particle per steradian per square meter per second for every 0.1 logarithmic energy bin, in units of $GeV/m^2.sr.s$. Trivially, one must multiply by the number of particles per unit area per steradian per second in their bin to get the total energy flux at each altitude bin for a given spectral form. To input this data into the NGSFC code the energy at each altitude must be added over all energy levels, creating a 1-dimensional data set of total energy deposition flux

at each altitude.

The general purpose table has 51 columns as mentioned above and 21 rows of bin size 50 $g\ cm^{-2}$ each. The table displays the ionization yield function in units of ion pairs per meter square per steradian per second. Total number of ion pairs for a given spectrum can be obtained by the method mentioned above.

As mentioned previously, the NGSFC code takes ionization energy flux in a 2-dimensional format using altitude and latitude. The data is now in 1-dimension with respect to altitude, so the user must create a latitude component. The NGSFC code has 18 latitude bins ($90^o - 80^o, 80^o - 70^o, 70^o - 60^o$ etc). For an isotropic flux, the same flux is entered for each latitude bin. The final data file to be input into the NGSFC code should now be a 2-dimensional set of ionization energy flux deposition at the 18 latitude bins for 46 altitudes, a total of 828 data points. For a point source, the input into latitude bins may be adjusted by the appropriate factor, including a correction for the $cos\ \theta$ factor as in [114]. This may result in hemispheric differences in the results.

The energy flux data as a function of altitude and latitude, generated as described above, may be used in the NGSFC code by way of a simple read-in subroutine. Depending on the units of the spectrum used, conversion to $cm^{-2}s^{-1}$ may be necessary since the NGSFC code uses cgs units. In order to

use the input as a source of NO_y, the energy flux must first be converted to ionization flux. This is accomplished using 35 eV per ion pair [95], which finally gives values in units of $ions\ cm^{-2}s^{-1}$. Constituents in the code are stored with units of number $cm^{-3}s^{-1}$. Therefore, the area ionization rate is converted to a volume rate using the height of the altitude bins, which depends on the current density of each bin at read in (the density depends on temperature, which depends on the presence of sunlight, etc.). This ionization rate is then used as a source for NO_y, assuming 1.25 molecules are created for each ion pair [95]. The model then runs as usual, incorporating this source of NO_y in the relevant chemistry computations. The general procedure here is the same as that used in previous work with both photon and solar proton ionization sources [62, 114].

It must be noted that alpha particles were not considered to produce these tables. At such high energies, an alpha particle can be approximated by four protons with the same energy per nucleon and the resulting ionization can be computed using the data generated with protons.

3.3 Comparison with existing simulations

We have compared our simulation with existing simulation generated in a previous work using CORSIKA [117] as well as analytical methods proposed

by Velinov et al. [119] (Table 3.3).

We found very good agreement with Usoskin et al. simulation [117] at 1 TeV (figure 3.3), 100 GeV (figure 3.4) and 10 GeV (figure 3.5). However, there is about 5% higher ionization in our simulation at lower altitudes. This can be attributed to the UrQMD model we have used, which is more efficient in tracking muons compared to FLUKA used in the earlier work. Since muons are a major source of atmospheric ionization, especially near the ground, we would expect this enhancement. It must also be noted that we used the latest version of the code (CORSIKA 6.900, 2009) compared to CORSIKA 6.204 (2005) used in the earlier work.

We also compared the shower profile at 1 PeV (figure 3.6) with Tanguy Pierog's (CORSIKA developer) simulation generated by the same hadronic interaction models and found very good agreement. This simulation provides the energy deposition profile of a 1 PeV primary using the EPOS-UrQMD hadronic interaction models produced with CORSIKA.

The analytical method [119] can be used for a thin target, which is above 50 km altitude. It uses the Bethe-Bloch solution to calculate ionization from proton propagation in the upper atmosphere. Also, the equation used to calculate ionization limits the primary energy range to 600 MeV - 5 TeV. We applied the analytical solution to the energy range of 17 GeV - 5 TeV in order

to ignore the effects of solar modulation. Our values of ionization are about 5% higher than predicted by the approximation (Table 3.3). As discussed earlier, CORSIKA does not allow altitude bins smaller than 1 $g\ cm^{-2}$, which contains the entire atmosphere above 50 km, and therefore, it is not possible to resolve different levels within 1 $g\ cm^{-2}$ bin, which explains the 5% difference.

Atmospheric ionization produced by the primaries in our energy range is a very tiny fraction of the total ionization from the GCR flux, and therefore we can not compare our results with certain models [120], but it will be possible to compare for a given CR spectrum.

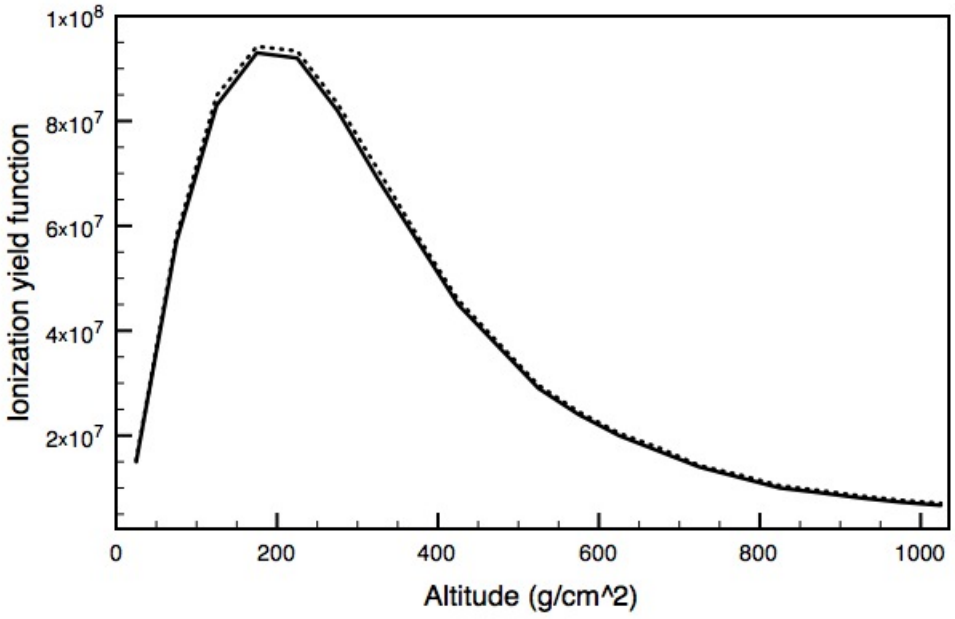

Figure 3.3: Comparison of our simulation (dash) at 1 TeV with Usoskin et al. (solid) [117].

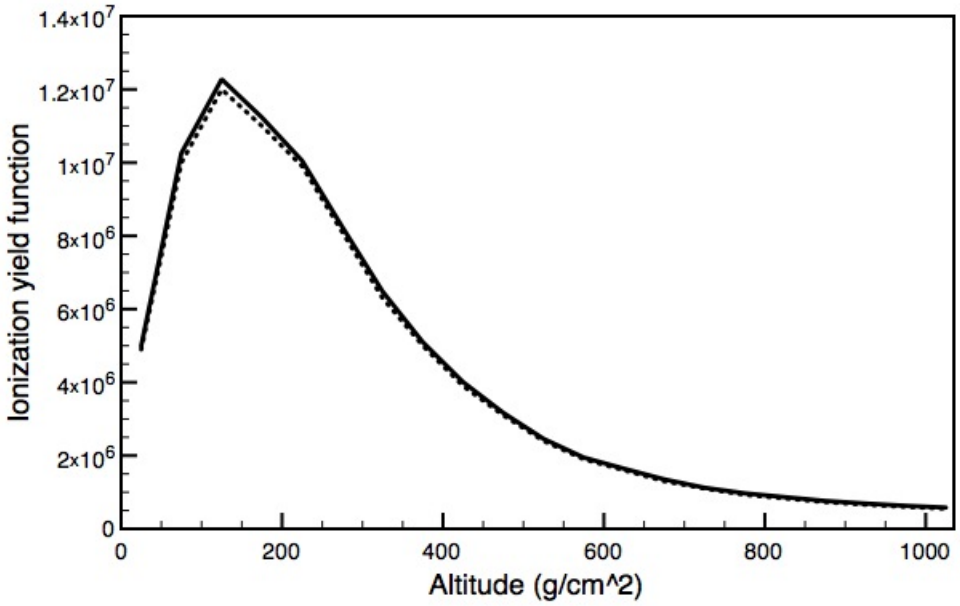

Figure 3.4: Comparison of our data (solid) at 100 GeV with Usoskin et al. (dash) [117].

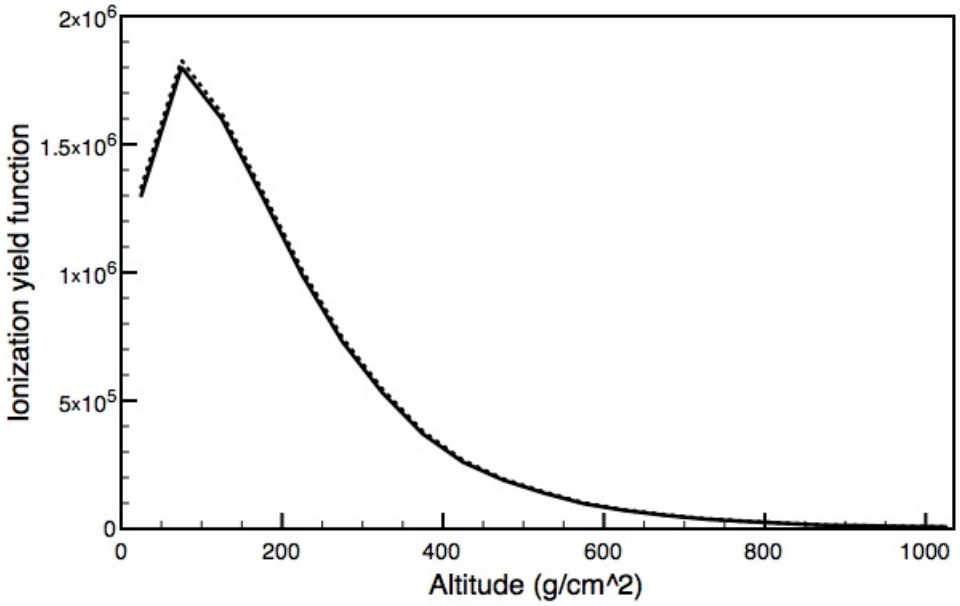

Figure 3.5: Comparison of our data (dash) at 10 GeV with Usoskin et al. (solid) [117].

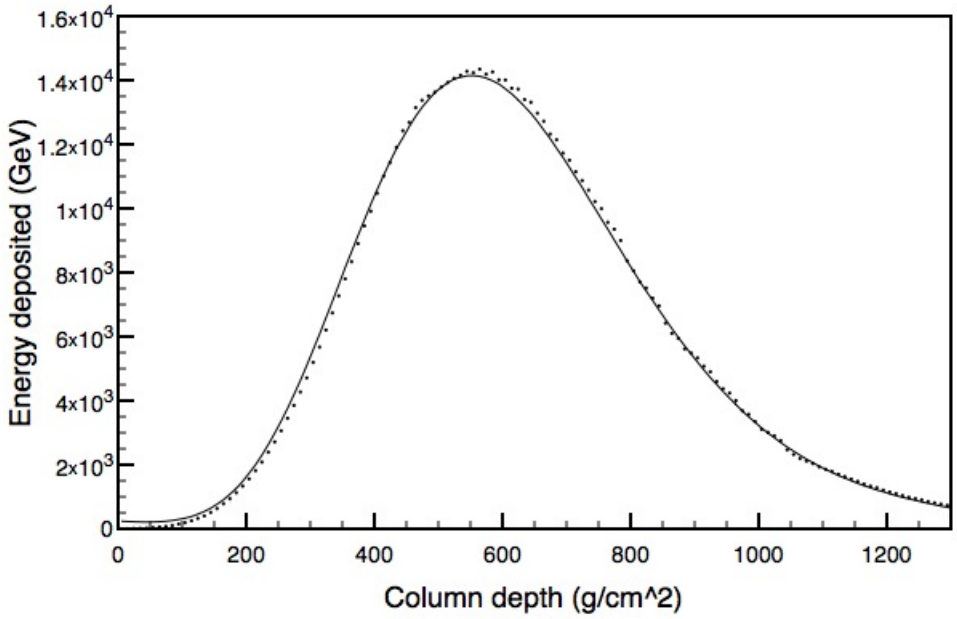

Figure 3.6: Comparison of our data (dots) at 1 PeV with T. Pierog's data (solid) produced with CORSIKA/CONEX in bins of 10 $g\ cm^{-2}$

Name	Value	Description
RUNNR	x	run number x = integer number to help keep track of runs
NSHOW	15	number of showers to generate
PRMPAR	14	Primary Particle, 14 = proton
ESLOPE	-2.7	slope of primary energy spectrum (irrelevant in our model because we use single energy level)
ERANGE	X X	Energy range of particle (GeV) X = Energy of Particle (Table 2)
THETAP	70 70	range of zenith angle (degree)
PHIP	-180. 180.	range of azimuth angle (degree)
SEED	x 0 0	random number sequence 1
SEED	x 0 0	randon number sequence 2
OBSLEV	0.	Observation level (cm)
ECUTS	.3 .3 .00005 .00005	Energy to cut off secondaries
MAGNET	20.0 42.8	Magnetic field centr. Eurpoe
HADFLG	0 0 0 0 0 2	Flags hadr interact & fragmentation
MUADDI	T	Additional infor for muons
MUMULT	T	Muon multiple scattering
ELMFLG	F T	em. interaction flags (NKG,EGS)
STEPFC	1.0	mult. scattering step length fact.
RADNKG	200.E2	outer radius for NKG lat.dens.distr.

ARRANG	0.	rotation of array to north
MUADDI	T	Additional muon information
LONGI	T 1 T F	V step 10
EPOPAR	input ../epos/epos.param	initialization input file for epos
EPOPAR	fname inics ../epos/epos.inics	initialization input file for epos
EPOPAR	fname iniev ../epos/epos.iniev	initialization input file for epos
EPOPAR	fname initl ../epos/epos.initl	initialization input file for epos
EPOPAR	fname inirj ../epos/epos.inirj	initialization input file for epos
EPOPAR	fname inihy ../epos/epos.ini1b	initialization input file for epos
EPOPAR	fname check none	dummy output file for epos
EPOPAR	fname histo none	dummy output file for epos
EPOPAR	fname data none	dummy output file for epos
EPOPAR	fname copy none	dummy output file for epos
ECTMAP	1.E2	Cut on gamma factor for printout
MAXPRT	5	Max. number of printed events
DIRECT	/data/dimitra/	Output directory
DATBAS	F	Write .dbase file
USER	you	User
PAROUT	F F	
DEBUG	F 6 F 1000000	Debug flag and log unit for out
EXIT		End input file

Table 3.1: Input File for CORSIKA - Complete Description of Variables at [58]

Number of Bin	Pressure (mb)	Approximate Altitude (km)
1	879	0
2	661	2
3	498	4
4	374	6
5	282	8
6	212	10
7	160	12
8	120	14
9	90.3	16
10	68.0	18
11	51.1	20
12	38.5	22
13	29.0	24
14	22.8	26
15	16.4	28
16	12.3	30
17	9.28	32
18	6.98	34
19	5.26	36
20	3.96	38
21	2.98	40
22	2.24	42
23	1.68	44
24	1.27	46
25	0.954	48
26	0.718	50
27	0.540	52
28	0.406	54
29	0.306	56
30	0.230	58
31	0.173	60
32	0.130	62
33	0.0980	64
34	0.0738	66
35	0.0555	68
36	0.0418	70
37	0.0314	72
38	0.0237	74
39	0.0178	76
40	0.0134	78
41	0.0101	80
42	0.00758	82
43	0.00571	84
44	0.00429	86
45	0.003230	88
46	0.002430	90

Table 3.2: Altitudes for NGSFC code.

Pressure (mb)	altitude (km)	q (cm-3*s-1) - CORSIKA	q (cm-3*s-1) - Analytical
0.00243	90	3.3651E-07	3.20293E-07
0.00323	88	4.47984E-07	4.2574E-07
0.00429	86	5.94377E-07	5.65456E-07
0.00571	84	7.90984E-07	7.52623E-07
0.00758	82	1.05024E-06	9.99104E-07
0.0101	80	1.39941E-06	1.33126E-06
0.0134	78	1.85701E-06	1.76623E-06
0.0178	76	2.4665E-06	2.34618E-06
0.0237	74	3.28368E-06	3.12385E-06
0.0314	72	4.35093E-06	4.13877E-06
0.0418	70	5.79227E-06	5.50957E-06
0.0555	68	7.69022E-06	7.31534E-06
0.0738	66	1.02257E-05	9.72743E-06
0.098	64	1.35793E-05	1.29172E-05
0.13	62	4.50311E-06	4.28376E-06
0.173	60	5.99267E-06	5.70069E-06
0.23	58	7.96703E-06	7.57896E-06
0.306	56	1.05996E-05	1.00833E-05
0.406	54	1.40635E-05	1.33785E-05
0.54	52	1.87052E-05	1.77941E-05
0.718	50	2.48711E-05	2.36595E-05

Table 3.3: Comparison of analytical approximation vs CORSIKA data for a thin target [119].

Chapter 4

Modeling high-energy cosmic ray induced terrestrial muon flux

4.1 Cosmic ray muons

Since muons traverse the atmosphere practically unhindered because of their small cross section, they provide a wealth of information about the energy of the primary particle. Muon detectors are cheap and are spread at a number of locations around the world. The shower propagates down towards the ground with the shower-front shaped like a pancake. Most of the energy of the primary particle is used up in ionizing the atmosphere. This component ionizing the atmosphere consists of charged particles and photons, also referred to as the electromagnetic component of the shower. A large fraction of this electro-

magnetic component is absorbed within the first 1000 $g\ cm^{-2}$ of atmosphere and mostly the hard component (muons) of the shower is able to reach the ground. This is very close to the ground for vertical showers and much higher in the atmosphere for inclined ones. Other particles and photons reaching the ground are not biologically effective. This atmospheric ionization induced by HECR primaries has already been modeled for energies up to 1 PeV [6] and described above (Chapter 3). Along with ionizing the atmosphere, secondary particles reach ground level. Depending on their energy, they have the ability to penetrate deep underground and into water. Not all secondary particles are biologically effective. For this study, we concentrate on the penetrating radiation component due to muons. Other particles such as low energy electrons, photons and alpha particles are not penetrating. Enhanced levels of secondary muon flux could be harmful to living organisms [23] by increased mutation rates, cancer and birth defects [64].

Muons are generated by the decay of charged pions and have a very small interaction cross section. Also, their cross section is a very weak function of energy and the ionization energy loss is a very small fraction of the primary energy, even at very high energies. As a result, high energy muons generated by high energy primaries hit the ground practically unhindered. But since muons are charged particles, they are easy to detect and give a dominant signal deep

in the atmosphere and underground. They are usually detected with detectors buried a meter or more underground in order to absorb the electromagnetic component.

The muon component dominates the flux of particles on the ground at energies above 100 MeV. Its contribution is about 85% of the total equivalent biological dose by cosmic rays [2,87]. At lower energies, the muon flux decreases because of their short lifetime of 2 μs. Muons with higher energy travel with higher velocities and hence travel longer distances due to the time dilation effects. They lose energy due to ionization at a rate of about 2 MeV per g cm^{-2}. Since the column density of our atmosphere is about 1000 g cm^{-2}, a muon loses around 2 GeV of energy, on average, upon reaching the ground (falling vertically). This radiation dose from muons at the ground level will be in addition to the dose from other components discussed elsewhere [66, 67].

Analytical models [44] can approximate muon flux resulting from vertical GCR primaries and a vast amount of data [56] is available from detectors around the world. Other methods can be used to calculate muon flux for the normal cosmic ray spectrum [28, 121]. But no model is available to compute muon flux when the CR primary flux is different from the normal GCR flux. In particular at higher energies, the hadronic interaction cross sections are only estimates, and reasonable predictions can be obtained only by computational

methods.

We have developed a lookup table to compute the terrestrial flux of muons resulting from high energy cosmic ray interactions with the atmosphere that can be used by convolving with the spectrum from any astrophysical source.

4.2 Description of modeling

We used CORSIKA to simulate air showers for a flat spectrum of high-energy primaries (protons) so that any arbitrary CR spectra can be applied later on, to calculate the muon flux.

In order to obtain data that is independent of the primary GCR spectrum and geographic location on the Earth, we simulated showers at fixed primary energies. The flux of muons at the ground level strongly depends on the zenith angle of the primary; therefore we simulated showers for a range of zenith angles. We compiled data for primaries from 10 GeV up to 1 PeV in 0.1 $\log_{10}$ intervals. At each energy, simulations are performed at zenith angles starting from 5, 15...up to 85 degrees. We averaged 90,000 showers at each energy for 10 GeV - 1 TeV range, 9,000 for 1 TeV - 10 TeV, 900 for 10 TeV - 100 TeV and 180 showers for 100 TeV - 1 PeV. Overall, the data is compiled from a large ensemble of 1.9×10^6 showers.

CORSIKA 6.960 was used for all the simulations. The code was set up with

EPOS as the high-energy hadronic interaction model due to its compatibility with KASCADE data. For low energies, the FLUKA hadronic interaction model was chosen since it is the fastest and best at tracking muons in our energy range [91, 93] The code was installed with the SLANT option to study the longitudinal shower development. It will be used for studying thermal neutrons in future. The CURVED option was chosen for primaries incident at large zenith angles and the UPWARD option for albedo particles. The energy cut was set at 300 MeV since it is adequate to get all the muons and hadrons produced by photon interactions while saving a significant amount of computing time. Sea level was set as the observation level.

CORSIKA outputs data on a number of particle species hitting the ground level. Each file contains momentum data of individual particles at the sea level from a single air shower. Muon momentum is extracted from each file generated by a primary at a fixed energy and fixed zenith angle. The momentum data is then compiled for all showers at a given energy and angle, and is binned in logarithmic energy bins of 0.1 GeV in $\log_{10}$ intervals. It is then normalized by the total number of showers, giving the muon flux from a single primary. As a result we get the terrestrial muon spectrum of a particular primary energy at a given zenith angle. Data obtained from different angles at a given primary energy is then averaged by $sin\ \theta$ weight resulting in an isotropic muon

spectrum at a particular primary energy. This is the data recorded in the data table. This process is repeated for all 51 primary energies from 10 GeV - 1 PeV.

As expected we get less muon flux at higher zenith angles (Figures 4.1 and 4.2). Low energy primaries are not efficient in producing muons of enough energy so that they can reach the ground. A large number of primaries at lower energies produce fewer muons at the ground level. The number of secondary particles produced in the shower increases with the primary energy and so does the number of muons hitting the ground (Figure 4.3). The contribution from larger zenith angle component is very small for low energy primaries, and goes up with energy. This is evident in Figure 4.3 where the flux from 100 GeV primary falls very steeply compared to primaries at higher energies.

Our primary energies are centered at 10 GeV, $10^{1.1}$ GeV and so on with bin size of 0.1 in $\log_{10}$ intervals. The number of particles in a given energy bin ($\frac{dN}{dE}$) can be calculated using the differential spectrum from any astrophysical source. This number is then multiplied by the data given in the table to get the corresponding muon spectrum for each primary energy. The total muon spectrum can be obtained by summing over a given energy range. Since the primaries higher than 17 GeV are unaffected by the geomagnetic field, their flux is independent of the geographic location. A large amount of literature

exists for muon flux for lower energies, both from experiments [56] or using approximate analytical methods [44].

4.3 Comparison with data

Let us now use these lookup tables to compare the results with existing data. Hebbeker and Timmermans [56] compiled all published data on muon flux from a number of experiments and made various corrections based on the detector altitude and geographical location. The data was then plotted together and fitted with a polynomial. This polynomial fit is considered to be a standard result to be compared to.

We have also compared the lookup table data with the Hebbeker and Timmermans polynomial fit to data collected from a number of experiments [56]. We find a maximum 15% deviation from the polynomial fit for low energy muons, 1-5% difference in the 10 GeV - 3 TeV range and an 8% deviation at higher energies. Overall it is a very good fit considering the experimental variation in data compiled in the reference [56] (Figure 4.4).

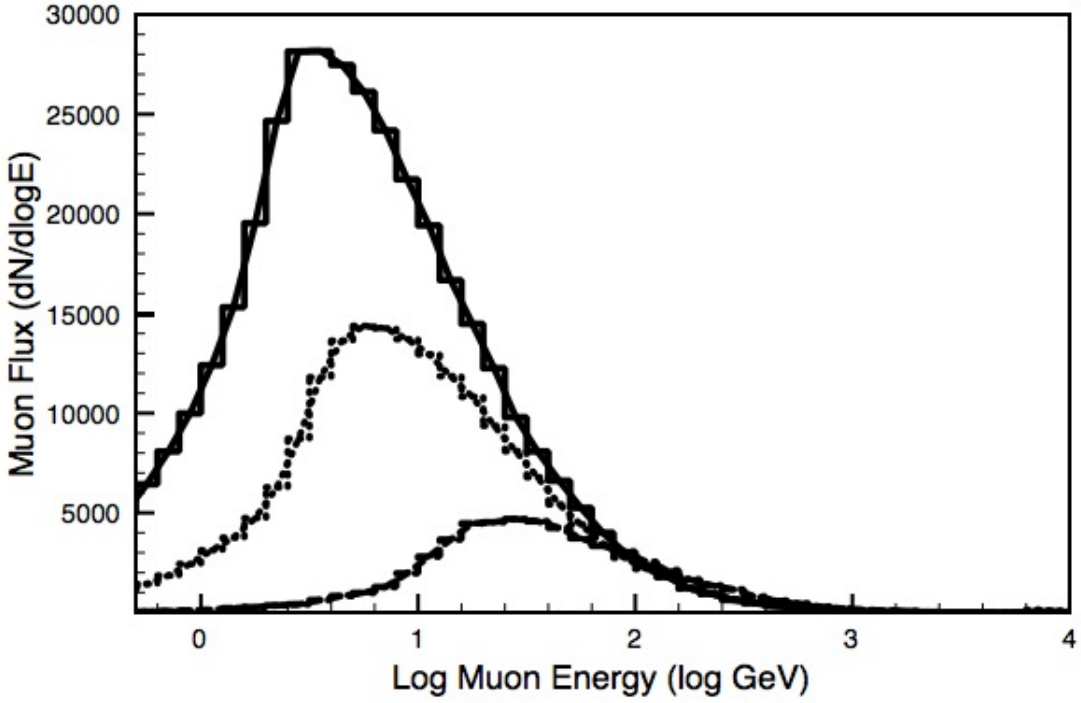

Figure 4.1: Differential muon flux for 10 TeV primaries at zenith angles 5^o (solid), 45^o (dotted), and 85^o(dashed). The flux goes down with increasing zenith angles [5].

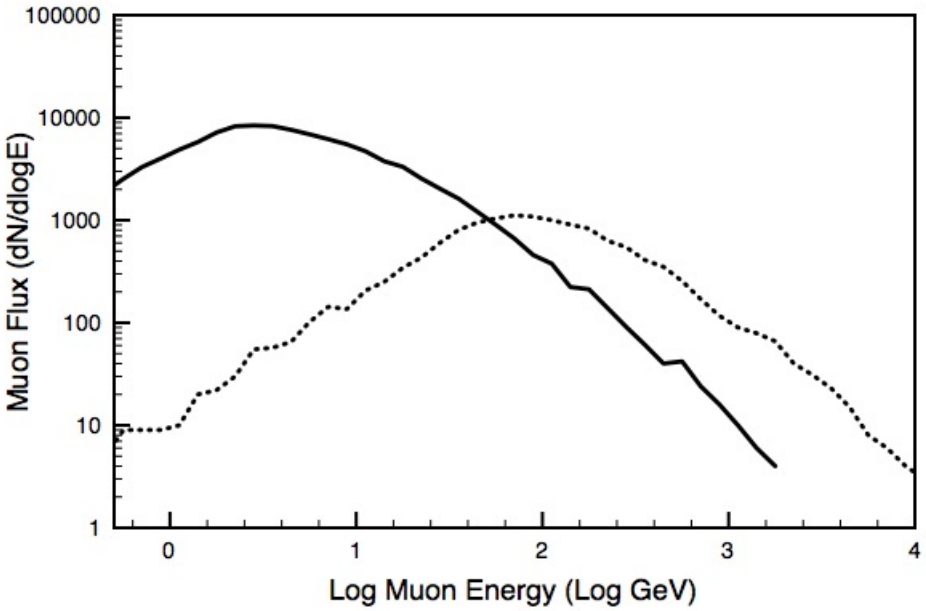

Figure 4.2: Differential muon flux for 1 PeV primaries at zenith angles 5^o (solid) and 85^o(dotted) [5].

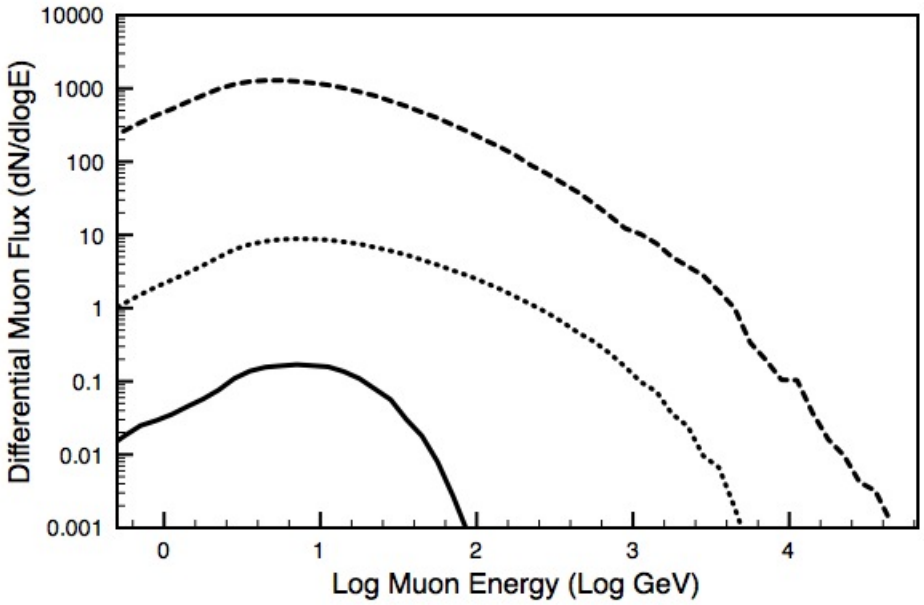

Figure 4.3: The muon flux averaged over the hemisphere from 100 GeV (solid), 10 TeV (dotted) and 1 PeV (dashed) primaries. Flux for higher energy primaries does not fall sharply compared to the lower energy primaries since the contribution from higher zenith angles increases with increasing primary energy [5].

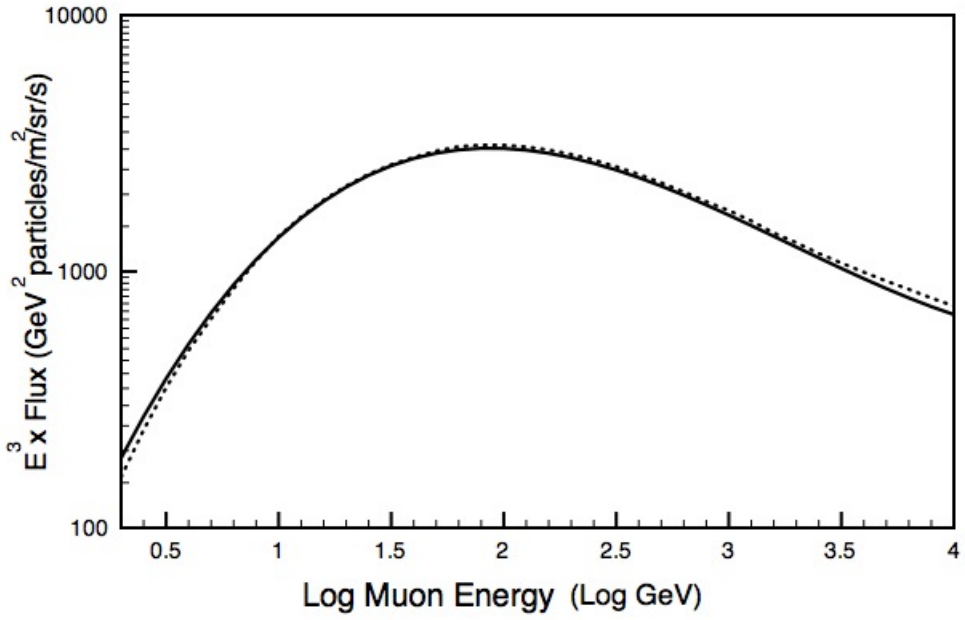

Figure 4.4: Muon flux computed from the lookup table (dots) compared with the Hebbeker and Timmermans (2002) [56] polynomial fit (solid) [5].

Results are presented in the form of lookup tables which present the muon flux as a function of primary energy. The primary energy is given at the top row and arranged in 51 columns going from 10 GeV up to 1 PeV. The first column gives logarithmic bins of muon energy at the ground. In order to evaluate the muon flux from a given cosmic ray spectrum, one needs to convolve the spectrum with this table. The spectrum will give the number of particles falling per unit area per second on the top of the atmosphere and this table will give the muon energy distribution in the same units.

Chapter 5

Terrestrial effects of enhanced cosmic rays from the extragalactic shock model

5.1 Biodiversity cycles and Cosmic Rays

A ~ 62 My periodicity in terrestrial biodiversity has been found in independent studies of paleobiology databases going back to 500 My [21, 78, 82, 100]. The physical cause driving this biodiversity cycle is not known. The period and phase of this biodiversity cycle correlates with the motion of our solar system in the galactic disk. Our solar system oscillates perpendicular to the galactic plane with an amplitude of about 70 pc and a period of 63.6 My [48]. It has been hypothesized [77] that the coincidence of time and phase of these two seemingly unrelated phenomena may not just be a coincidence, but are related

by the following proposed mechanism. The Milky Way is falling toward the Virgo cluster at the rate of 200 km/s due to its gravitational pull. A galactic shock is formed at the north end of our Galaxy due to this motion. Such a shock is capable of accelerating particles and exposing our galaxy's northern side to a higher flux of cosmic rays. The earth is protected from these cosmic rays by the galactic magnetic field when it is within the galactic disk or at the southern side. But as it moves up the galactic plane, the magnetic field weakens and as a result it is exposed to an enhanced flux of high energy cosmic rays. This happens once every $\sim 62\ My$ when we are at the north with higher cosmic ray exposure and the biodiversity declines at this time. Such an exposure will persist for about 10^7 years in each cycle [77, 79].

The spectrum of extragalactic cosmic rays hitting the Earth's atmosphere has already been calculated [77]. The flux as a function of displacement from the galactic plane, z, is given by

$$F(z,E) = C_n\{{E_p}^{-2.7} e^{\{-\frac{E_p}{3}^{1/2}\}} + f(z){E_p}^{-3.2} e^{(\frac{-E_0}{E_p})}\} \tag{5.1}$$

C_n is a normalization constant, $f(z)$ parametrizes the cosmic ray enhancement due to the solar position, E_p is the energy in PeV, E_0 is the variable cutoff in PeV.

When, $E_0 = 3PeV$ and $f(z) = 1$, the first term gives the normal, low en-

ergy cosmic ray flux by sources within the Galaxy. The range of flux enhancements can be estimated that are consistent with the extragalactic backgrounds etc described in detail here [77, 79]. Lowest flux in the range is obtained by setting $E_0 = 10^{-3}$ and will be called case 1. Highest flux is calculated by setting $E_0 = 10^{-4}$, and will be called case 2 in this manuscript. The parameter $f(z)$ is adjusted such that flux at 1 TeV is enhanced by a factor of 4 in case 1 and by a factor of 25 in case 2.

We calculate the magnitude of various terrestrial effects from such an exposure and discuss their impact on the biosphere to answer whether this mechanism is capable of driving biodiversity cycles.

5.2 Terrestrial effects

In this section, we discuss three terrestrial effects impacting the biosphere.

- Enhanced atmospheric ionization from cosmic rays depletes the ozone layer and lead to increased UVB flux on the ground
- Enhanced atmospheric ionization from cosmic rays could lead to cloud cover changes and have climatic implications, and
- Enhanced flux of secondary muons can directly cause biological damage on the ground.

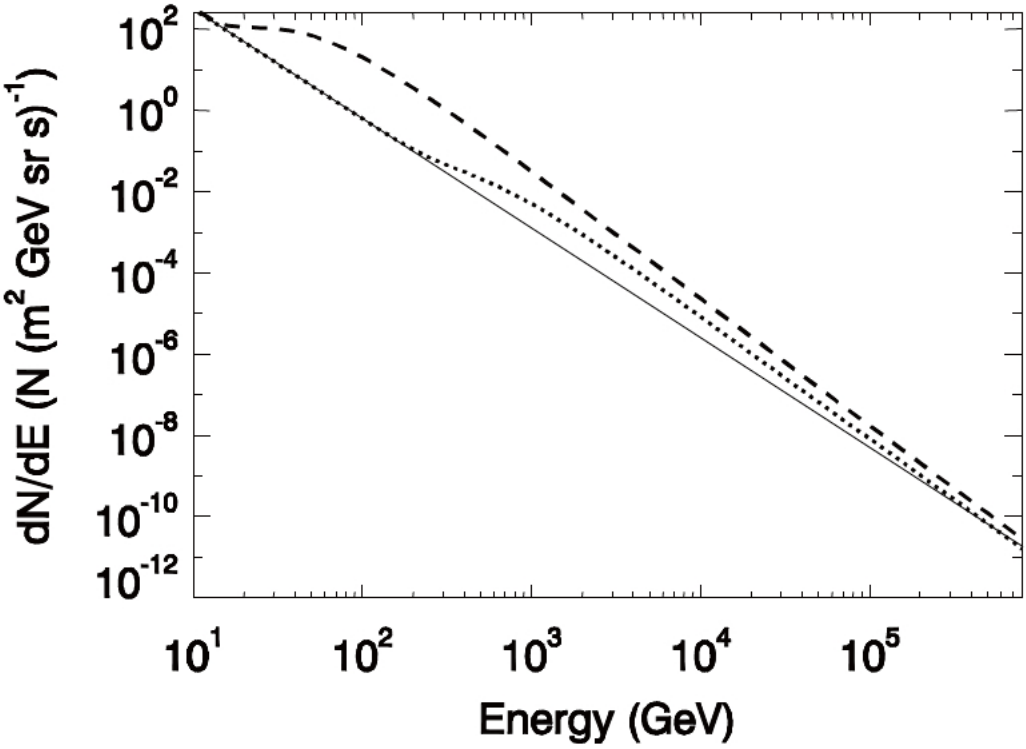

Figure 5.1: Enhanced cosmic ray spectra from the extragalactic shock model [77,79]. The dotted curve represents case 1 (minimal estimate) and the dashed curve represents case 2 (maximal estimate).

5.2.1 UVB damage from ozone depletion

Figures 5.3 and 5.4 show the energy deposition profiles obtained by CORSIKA simulations. The number of particles increases as the shower progresses depositing more energy in the atmosphere, as seen in the figure. As the number of particles increases, the energy of individual particles decreases and reaches a threshold below which no more new particles are produced in the shower. This feature can be seen in the declining part of the energy deposit curve (Figure

5.2). As expected, the peak of the higher energy primary is located deeper into the atmosphere.

Let us now go into more detail on how atmospheric ionization from cosmic rays affects the atmospheric chemistry. Our atmosphere consists primarily of N_2 (80%) and O_2 (19%) along with traces of other gases. This electromagnetic energy deposited in the atmosphere ionizes N_2 and O_2 molecules starting a series of molecular reactions. The triple bond of N_2 is broken, leading to the formation of a number of compounds such as NO and NO_2, referred as NO_x, present in very low abundance in the present atmosphere. NO_2 is a brown gas and may have opacity effects. But since the production of NO_2 in the atmosphere is in small amounts, this effect will become significant only in extreme cases.

NO_x compounds catalyze the conversion of O_3 to O_2 through several catalytic reactions. There are a series of other photochemical reactions due to enhanced ionization involving a number of other species such as oxygen, nitrogen, hydrogen, chlorine and bromine. A detailed description of all the photochemical reactions can be found here [112].

NO_x compounds react catalytically in the following way to deplete ozone:

$$NO + O_3 \rightarrow NO_2 + O_2$$

$$NO_2 + O \rightarrow NO + O_2$$

Net reaction is the following:

$$O_3 + O \rightarrow O_2 + O_2$$

Ozone is depleted to oxygen in the stratosphere and gives way to the solar UVB (280-315 nm) flux [101]. The wavelength range of UVB radiation is strongly absorbed by DNA and can damage it, leading to a number of harmful effects. Harmful effects of UVB also include erythema (sunburn), skin cancer and mutations leading to other diseases. An increase in flux of UVB can be harmful to a variety of organisms such as phytoplankton which form the base of the aquatic food chain.

Using the ionization lookup tables, we calculated the atmospheric ionization profiles resulting from enhanced cosmic ray exposure in the extragalactic shock model. These ionization values served as an input to the NGSFC code described previously. Photochemical simulations were performed by Brian Thomas and all the details are reported here [79]. Ozone depletion from our minimal assumption (case 1) was found to be much smaller than the current depletion rate from anthropogenic causes. For the maximal assumption in cosmic ray flux (case 2) the globally averaged ozone depletion was about 6%, which is twice due to anthropogenic causes, which is about 3%. None of the two values are capable of causing any serious damage to the biosphere. This was expected since most of the energy is deposited much lower in the

atmosphere and ionization increase in the upper atmosphere is very small.

Apart from these effects, an increase in atmospheric ionization could enhance cloud formation and hence increase the low altitude cloud cover [75, 76]. An increased cloud cover would enhance the albedo which would result in less solar energy on the ground, decreasing the global temperature.

5.2.2 Cloud cover

There is some evidence that cosmic ray induced atmospheric ionization could enhance the low altitude cloud cover [34, 54, 55, 109]. Although the study of cloud microphysics associated with atmospheric ionization is still in its infancy, preliminary experimentation suggests a correlation between the atmospheric ionization and aerosol formation [31] that directly affects the cloud formation rate. This ionization change will affect the global ionosphere-earth current density J_z, which has effects on cloud microphysical processes such as electroscavenging and ion mediated nucleation [116]. The change in ionization from the cosmic ray variability has been previously computed for a solar cycle, which indicates a linear relationship between ionization and the low altitude cloud cover [118]. However, other studies [35, 70, 106] show a much smaller effect on the low altitude cloud cover. They are either unable to find a correlation or estimate a small fraction of contribution to the total change in cloud

cover from galactic cosmic rays. Recent work by Lockwood et al. [73] attributes the recent colder UK winter to a lower solar irradiance and an enhanced flux of galactic cosmic rays. We note that the cosmic rays in the extragalactic hypothesis [77] are of higher energy, and will penetrate deeper in the atmosphere [6] producing more ionization and hence should have a greater effect than the galactic cosmic rays.

Muons are the primary source of atmospheric ionization at low altitudes. With an enhancement of HECR flux, there will be an increase in the flux of high energy muons at low altitudes, thereby enhancing atmospheric ionization there. This could lead to increased low altitude cloud cover resulting from HECR exposure predicted by the extragalactic shock model.

The enhanced spectra from the extragalactic shock model results in an increase in the flux of primaries up to about 1 PeV. Because of the uncertainty in the values of the magnetic field parameters in this model, it gives a range of possible results. Here, we explore the maxima and minima of HECR exposure obtained from the model. As shown in Fig 1, the minimum flux (case 1) has the flux enhanced by a factor of 4 at one TeV and by a factor of 25 for the maximum flux (case 2). The normal atmospheric ionization values corresponding to lower energies are calculated using an existing ionization table [117]. Atmospheric ionization profiles at the pole corresponding to different

cosmic ray inputs are shown in Figure 5.2. We concentrate on the increase in ionization from these two cases at an altitude of 3 km ($\sim$ 700 gcm^{-2}), where most low altitude clouds reside.

We compared the values of atmospheric ionization from the two cases with that at the time of the cosmic ray maxima in a solar cycle. Looking at the total energy deposited in the atmosphere, case 1 has a global enhancement factor of 3.2 and case 2 a factor of 30.7. Global enhancement is by 28% in a solar cycle. But most of the ionization is above 10 km altitude and the enhancement at lower altitudes is much lower, as expected. At the 3 km level (Figure 5.3), for case 1 (minimal), we found an average increase in ionization of 38% with 79.6% enhancement at the equator and 20.4 % at the poles. For case 2 (maximal), the average enhancement was by 600%, with 770% at the equator and 532% at the poles at 3 km altitude. The average increase in ionization at 3 km altitude in a solar cycle is 4.2%. Ionization increase in the minimal case is about 9 times that of a solar cycle. Since higher energy primaries are unaffected by the geomagnetic field, one gets almost the same flux of particles globally. When compared to the normal GCR flux, the difference at the equator is much higher than at the poles because the normal particle flux at the equator is much lower than at the poles. For case 2, the flux of high energy primaries is even higher, which translates to an increase in the flux of high energy muons.

High energy muons, because of their very small cross sections, can penetrate deeper into the atmosphere increasing ionization in the lower atmosphere. As discussed above, the correlation between ionization and cloud cover is not well quantified and estimates of the contribution of cosmic rays to cloud cover changes varies from 0 to 100%. Due to the absence of a quantitative model to calculate cloud cover changes from increased ionization, accurate estimates of cloud cover changes are not possible. However, it would be safe to predict that the magnitude of cloud cover change with this long term cosmic ray variability would be much greater than the changes during a solar cycle.

This large difference in our estimates of ionization (case 1 and 2) is due to the large uncertainty in the HECR flux calculated from the extragalactic shock model. For the minimal case, the expected change in cloud cover is probably not enough to cause a significant global temperature change. On the other hand, the expected cloud cover change from the maximal case could be large due to a significantly increased estimate of ionization and can certainly lead to a drop in the global temperature and increase in precipitation. The actual cloud cover change can be anywhere between the two cases discussed here. As with earlier ozone depletion computations [79] the estimates of effects that may impact biodiversity appear in this case to span the range from unimportant to serious.

An interesting aspect of this question concerns strontium isotope ratios. Melott et al. [80] have noted a strong 62 My periodicity in the fluctuations of the 87Sr/86Sr ratio, with the sense that this ratio rises when biodiversity drops. Such an increase would typically be associated with uplift. Melott et al. [80] have discussed some of the evidence suggesting that climate change can affect uplift. A recent study [84] suggests a $\sim$ 56 My periodic cycle in North American sedimentation during this period. Also, Li et al. [72] have argued that there should be a strong temperature effect due to erosion rates of mica, raising this isotope ratio for cooler temperatures. Melott et al. [80] speculated that this effect might provide a link between the natural oscillation frequency and phase agreement of the extragalactic shock scenario and geoisotope data that is synchronous with the biodiversity signal.

More accurate computations of the various terrestrial effects from cosmic rays will be possible in the future with better measurements of parameters used in the extragalactic shock model and especially with improvement in the understanding of cloud microphysics. A better quantitative understanding of cloud cover changes from long term cosmic ray variability in future will provide us with a better picture of the possible long term climate change and its impact on the biosphere.

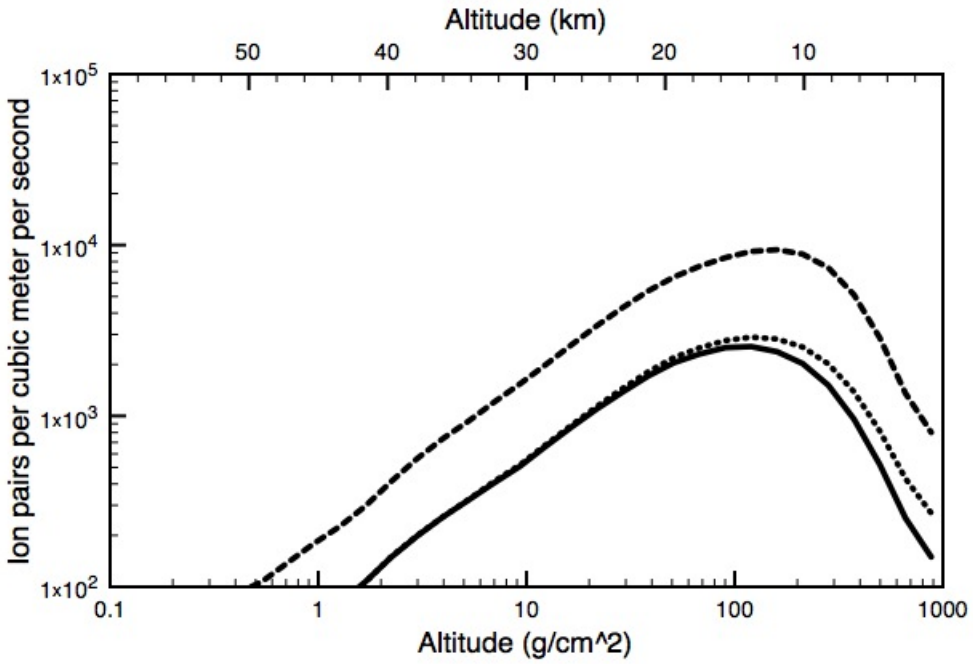

Figure 5.2: Atmospheric ionization as a function of altitude at the poles from various cosmic ray flux inputs. Maximal ionization (dash), minimal ionization (dots) and normal ionization at the pole from the normal cosmic ray maxima (solid line) in a solar cycle [7].

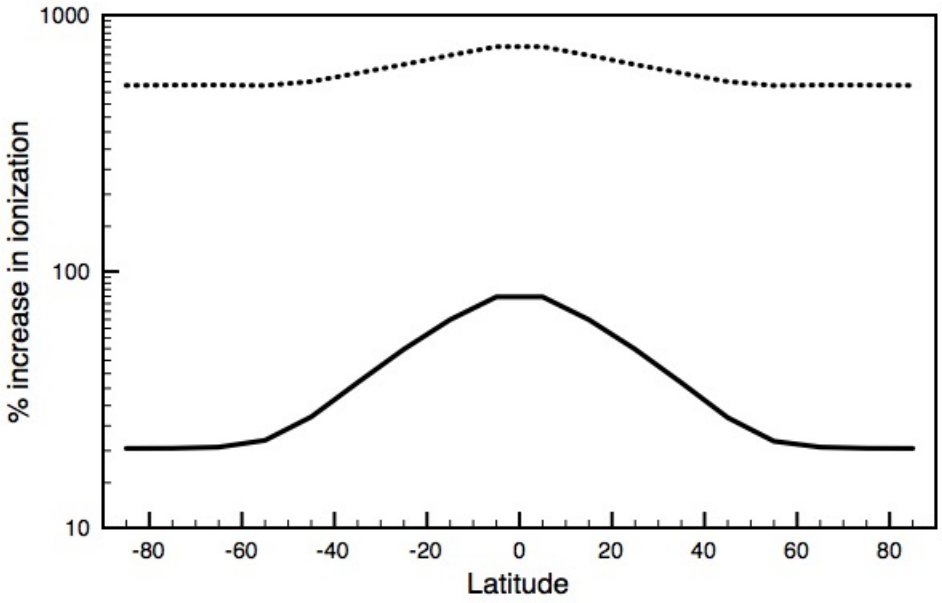

Figure 5.3: Percent increase in atmospheric ionization for case 1 (solid) and case 2 (dotted) at 3 km altitude. The enhancement is greater at the equator than the poles because the geomagnetic field guides the majority of normal cosmic rays toward the poles, while the cosmic rays in the extra-galactic model are typically too energetic to be redirected [7].

5.3 Biological damage from enhanced Muon flux

5.3.1 A brief review of radiation biophysics

Ionizing radiation, even though very small in energy compared to non-ionizing radiation, is very damaging to life. Of all ionizing radiation types, muons are the most penetrating and therefore dominate the radiation dose at the ground [87, 105]. The biological impact of cosmic rays has been studied primarily to evaluate the damage to the human body in air and space travel. A lot of research has been done in the context of space travel, in particular with regard to the future human mission to Mars [**?**]. Astronauts will not be protected by the Earth's extended magnetosphere and will be vulnerable to galactic cosmic rays and solar flares. Cosmic ray primary and secondary particles can easily penetrate bones and tissues. The impact of cosmic ray neutrons has also been studied on airline staff and found to be carcinogenic for elongated exposures. Studies [8, 51, 74, 96, 97] done on airline crews showed a significant increase in cancer rates compared to the normal. These particles can result in a significant biological damage depending on the type of particle and energy. A lot of experimental effort has been made in understanding the impact of this radiation in outer space for planning a good strategy for human space missions

in outer space. But such studies are of limited importance to assess the impact of cosmic rays on terrestrial life. As we have seen earlier, the flux of particles at the surface is dominated by high-energy muons and other lower energy components that are not as biologically effective. The impact of such muons on biological samples has not been studied so far. Experiments have been conducted to study the effect of keV muons on non-human biological samples, but such experiments cannot provide us with a quantitative understanding of the damage at higher energies. Damage can be estimated from theoretical modeling the propagation of such particles in biological samples and compare similar damage caused by other particles such as electrons. Higher energy muons are hard to produce in the laboratory. In order to conduct experiments with such muons, one needs to tap them from particle accelerators.

In normal circumstances, there is always some amount of biological damage caused by cosmic rays, but life has natural repair mechanisms that can repair some of the damage caused by normal dose of CRs. But in case the dose is increased, this repair mechanism can become inadequate which causes dangerous mutations leading to various diseases, including cancer.

Biological damage is quantified using experiments where a sample is exposed to different doses of radiation of different types. In biophysics literature, it is a convention to describe the dose of particles as radiation. For our case,

even though we will be talking about damaging effects of elementary particles, it will be named as radiation following this convention.

Absorbed dose, D is the amount of energy deposited in a unit mass of the material from ionizing radiation or $D = \frac{dE}{dm}$. Although it is a good measure to estimate the damage on a uniform sample, it does not work with biological samples. Biological samples are non-uniform both in terms of composition and density and different components of a cell respond in a different way to a given radiation dose. One can however apply this equation to a relatively uniform sample such as a specific tissue or an organ. The measure of the biological damage suffered by a tissue or an organ is given by the equivalent dose, H_R. Equivalent dose is given by:

$$H_R = w_R \times D_R \tag{5.2}$$

where D_R is the averaged dose absorbed by the organ R and w_r is the radiation weighting factor, also known as the quality factor. This quality factor is determined experimentally by exposing samples to different radiation types and comparing the relative damage.

Biological damage caused by radiation depends on the type of radiation and its energy. Equal doses of different radiation types result in different types of biological damage. This is because different radiation types interact

with matter in different ways and the magnitude of damage is a function of energy too. A good measure for measuring damage in a sample is the energy deposited per unit path length or Linear Energy Transfer (LET) for different radiations. LET or the stopping power is given by the well known Bethe-Bloch equation where the rate of energy deposition per unit length depends on the square of the charge of the particle and inversely proportional to the square of the velocity. The differential energy loss per unit length in keV/μm is given by:

$$\frac{dE}{dx} = \frac{40\pi e^4 z^2 NZ}{mv^2}[ln\frac{2mv^2}{I_0} - ln(1-\beta^2) - \beta^2] \tag{5.3}$$

Where e is the charge of the electron, v is the velocity of the particle, N is the number of atoms per unit volume in the medium, Z is the average number of electrons in the atom, I_0 is the ionizing potential of the medium, z is the charge of the ionizing particle and β is its velocity.

As the particle travels through the medium, it loses energy by ionization and hence its velocity goes down. This makes $\frac{dE}{dx}$ go up, until the particle loses its kinetic energy; and then $\frac{dE}{dx}$ drops, going towards zero until the particle stops. This is shown by the Bragg curve, where the maximum energy deposition occurs toward the end of the particle's trajectory in the medium, also known as the Bragg peak. It is at this peak where one expects maximum

damage from incident radiation.

Radiation ionizes the material it is passing through, and in case of biological matter, ionization removes electrons from the atoms that make up the molecule of a tissue and hence it falls apart. Quantitative analysis of biological damage is derived from these books [2, 68, 71].

In order to quantify the damage, each radiation type is assigned a radiation weighting factor, w_R or the quality factor which gives its relative biological effectiveness (RBE).

One would think that RBE would go up with LET because more energy deposited per unit path would result in more damage. However, when the energy deposited increases beyond a certain point, the ionization density is more than enough at critical points within a cell, thus wasting the energy without doing more damage, also known as overkill. As shown in figure 5.4, very high LET radiation is as effective as the low LET radiation due to this effect.

Overall, radiation damage depends on the following factors:

(1) Radiation Flux ($\Phi(E)$)

(2) Effective absorbed dose (D_R), which in turn depends on:

(a) Type of radiation (w_R)

(b) Type of tissue/organ exposed (w_T)

In order to estimate the dose from any radiation source, one needs to combine these factors.

Total effective dose is given by:

$$D_{Total} = \int \Phi(E).w_{FD}.dE \tag{5.4}$$

Where w_{FD} is the flux-to-effective dose conversion factor. Since producing muons to conduct experiments is very difficult, a number of theoretical studies have been conducted to calculate the conversion factor for muons on human samples. For muons, this conversion factor remains fairly constant with increasing muon energy [19, 38, 88]. Therefore, the damage does not depend specifically on the energy of the muon, but the overall flux. Also, $\frac{dE}{dx}$ for muons is a very slow function of energy [50] and ionization produced by very high energy muons increases modestly with energy.

5.3.2 Radiation dose from enhanced muon flux

Similar to the method employed to evaluate the atmospheric ionization values, we used the muon lookup tables to calculate the muon flux at the surface from the two cases. The flux obtained from the primary energy spectrum has already been compared with existing results and was in very good agreement. Flux

from case 1 shows a shift to higher energies as expected. The total energy deposition from muons was enhanced by 47% both because of the increased number of particles as well as the increased average energy of muons. For case 2, there is a much higher increase in flux and the spectrum shifts a bit further to higher energy muons. The total energy deposition in muons in this case was increased by a factor of $15.89 \sim 16$. We see a considerable increase in both the number of muons and also the average energy of muons. Under ordinary circumstances, muons contribute 85% to the biological dose from cosmic rays at the surface [87, 105]. Such an increase in flux will considerably increase the radiation dose and can be potentially harmful to the biosphere.

The effective radiation dose from muons is given by:

$$D_\mu = \int \Phi_\mu . w_{FD} . dE \tag{5.5}$$

Where Φ_μ is the muon flux on ground. We can use the muon flux calculated above for both cases and convolve with the flux-to-dose conversion factor. The flux-to-dose conversion factor has been theoretically determined for muons up to 10 TeV on human samples. To calculate the biological effects over the 500 My timescale, values for humans will not be useful and studies on non-human samples need to be conducted. But, studies do suggest that biological damage

is proportional to the overall muon flux, and the fluence-to-dose factor remains fairly constant with energy [19, 38, 88]. Therefore, we calculate the ratio of fluxes for muon enhancements in both cases in order to get an estimate of the biological damage.

$$\frac{D_{\mu_{Enhanced}}}{D_{\mu_{Normal}}} = \frac{\phi_{Enhanced}}{\phi_{Normal}} \tag{5.6}$$

For case 1, we saw a flux enhancement of 88% and for case 2 the enhancement was by a factor of 24.5. This would translate to an 88% increase in effective dose for case 1 and by a factor of 24.5 for case 2. Other components such as electrons and photons are already absorbed in the atmosphere and those reaching the surface in modest quantities are not biologically effective. Also, α particles are not penetrating and can be easily stopped by a thin sheet of paper or by our skin. Of the overall radiation from natural sources, cosmic rays contribute to about half of the effective dose from penetrating radiation [2]. The other half is contributed by terrestrial sources which are primarily from radionuclides of the uranium-thorium series. The contribution from cosmogenic radionuclides is very small and can be neglected.

5.3.3 Summary

Looking at the terrestrial effects discussed above, ozone depletion from enhanced UVB exposure is modest and will not have any significant contribution to biological damage. Cloud cover changes can not be determined due to the lack of knowledge of cloud microphysics and therefore this effect is of limited importance. Enhanced muons flux however directly affects living organisms and could be the primary mechanism capable of driving biodiversity decline. Increase in the background radiation dose can result in increased rate of mutations and carcinogenic diseases over a period of $\sim 10\ My$, when the cosmic ray exposure is highest.

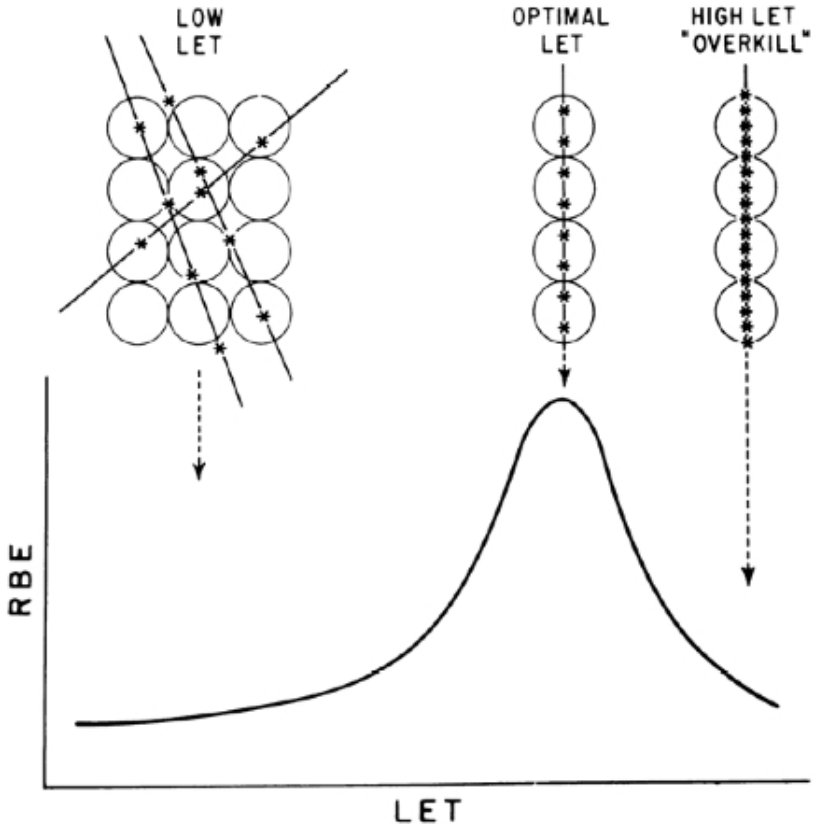

Figure 5.4: LET vs RBE. Circles shown above represent cells. If the energy is deposited on a number of critical points on a cell, the cell gets killed. Low LET radiation is inefficient because it does not produce enough ionization to attack all the critical points. High LET radiation on the other hand produces more than enough ionization, wasting the energy and hence is inefficient too. Optimal LET radiation produces just enough ionization to damage the critical points, and hence has the highest RBE [52].

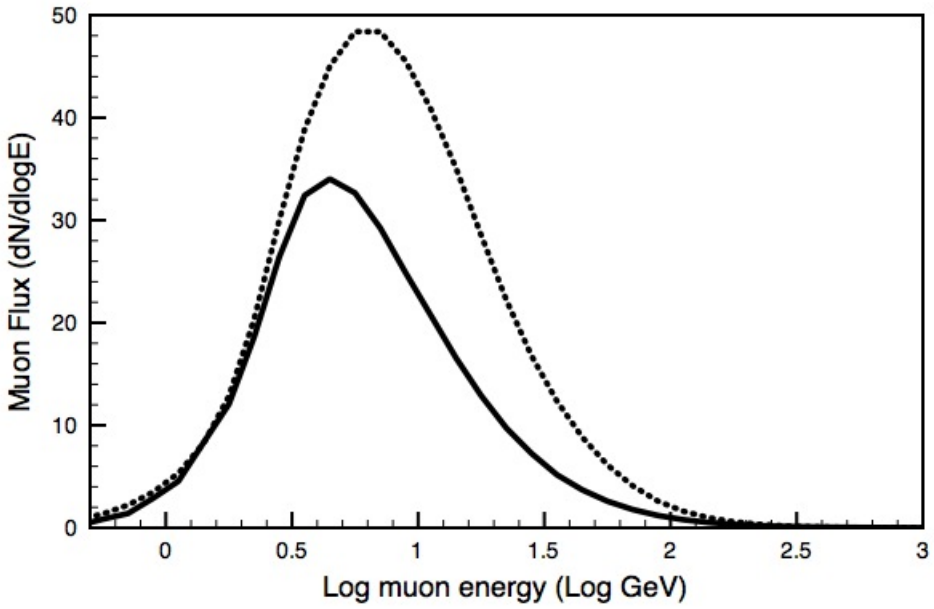

Figure 5.5: Enhanced muon flux (dots) from Case 1 in the extragalactic shock model compared with the normal muon flux (solid).

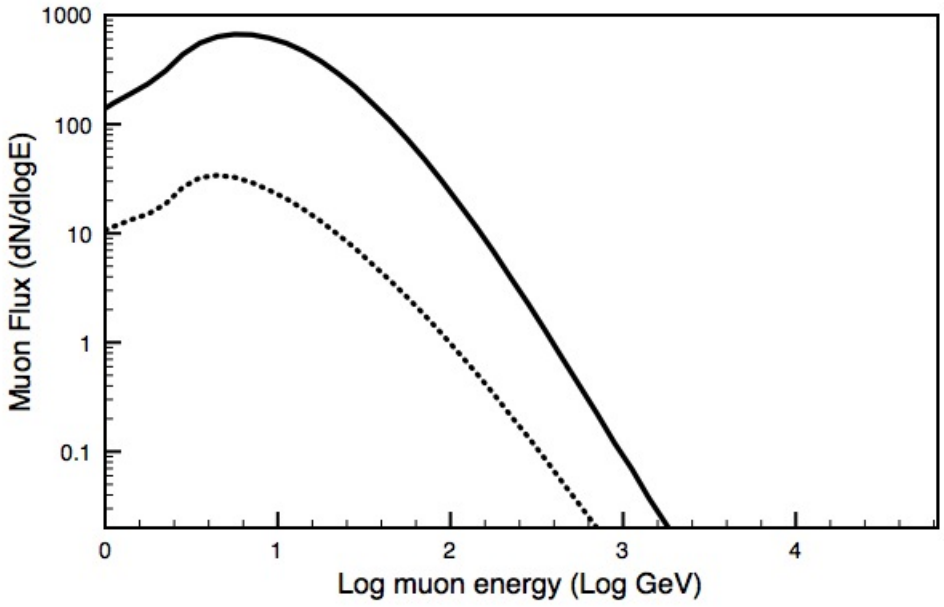

Figure 5.6: Enhanced muon flux (solid) from Case 2 in the extragalactic shock model compared with the normal muon flux (dots)

Chapter 6

Other applications and future work

6.1 Applications

Lookup tables developed to calculate the atmospheric ionization and muon flux can be used for other studies too. Obvious applications are studies of terrestrial effects from other intense astrophysical sources. Here we outline a few such applications.

6.1.1 Galactic Gamma Ray Bursts

It has been suggested that it is likely that the Earth has been hit by a GRB which had a significant effect on the biosphere. Detailed computational modeling of atmospheric effects of the photon burst gives a good estimate of the damage caused by such an event [112]. A burst pointed at Earth within 2 kpc can cause serious damage. There have been some observations [25] indicating the production of cosmic rays resulting from GRBs. Present models suggest that particles could be accelerated across the shock releasing ultra-high energy cosmic rays up to energies of $10^{18}\ eV$. However, the effects of cosmic rays were not taken into account in the previous analyses. The spectrum and flux of CRs on Earth resulting from a GRB has to be calculated. As mentioned earlier, we plan to extend our work to these energies so that effects of such high energy bursts could be estimated.

Some models suggest that Gamma Ray Bursts are capable of accelerating particles to ultra-high energies and are one of the sources of UHECRs observed on the Earth. If that is the case, the impact of UHECRs on the Earth would be substantial and could not be ignored as in previous analysis with photons. Apart from the uncertainty in the cosmic ray spectrum from GRBs, their composition is not well constrained at such higher energies. The biggest uncertainty apart from these two is the knowledge of interactions at

these energies. Currently, the development of air showers at such high energies is based on theoretical models. Interaction cross sections at these energies are not anticipated to be available in the near future either.

6.1.2 Nearby Supernovae

Estimates suggest that a supernova occurring within 10 *pc* will significantly damage the Earth's atmosphere. The estimated rate of supernovae within 10 *pc* is about 2 per *Gyr* [81]. When such an event occurs, there will be a flux of high energy cosmic rays accelerated by the SN blast wave. In the previous work, the atmospheric ionization due to the normal GCR flux was simply multiplied by a factor of 100 to account for CRs from nearby supernova. Normal GCR flux consists primarily of low energy protons which are easily deflected by Earth's geomagnetic field and hence are concentrated at the poles, and almost negligible flux at and near the equator. However, CRs generated from a supernova blast will be much higher in energy and will not be deflected by the geomagnetic field. As a result, one would see the flux distributed uniformly over the globe. Also, higher energy CR penetrate deeper into the atmosphere and their effects cannot be studied by simply enhancing the low energy flux as done previously. There are calculations of the CR spectrum in supernova remnants that can be used as an input for our analysis [11].

Galactic cosmic rays are thought to be produced by an acceleration mechanism of supernovae shocks. Models predict particle acceleration up to the PeV range from shock fronts. If such an event occurs nearby, the flux of cosmic rays from the shock is anticipated to be much higher than normal. The spectrum of particles entering the Earth's atmosphere needs to be determined. Such calculations will take into account the diffusion of particles and the nearby magnetic fields.

6.1.3 Extrasolar planets

Cosmic ray flux on exoplanets atmosphere has been calculated [49] and its astrobiological impact have been discussed qualitatively. Terrestrial effects from such cosmic ray exposure can be calculated using our methodology.

6.2 Future work

6.2.1 UHECRs

As described earlier, there is some evidence of UHECR production from GRBs [25, 26]. Previous study on the terrestrial impact of a galactic GRB was done ignoring UHECRs. We intend to extend our modeling to include the effects of UHECRs. Atmospheric ionization profiles can be obtained by CONEX [13,90],

which is another model to obtain atmospheric ionization profiles at ultrahigh energies. It is a one-dimensional Monte Carlo code where low energy sub-showers are treated numerically with hadronic cascade equations. This results in drastic reduction in computing time and a major improvement over the 'thinning' algorithm [57] used for ultra-high energy showers previously.

6.2.2 Thermal neutrons

Although CORSIKA does a good job in tracking muons and giving the electromagnetic energy deposition profile, it does not track neutrons below the energy of 50 MeV [57]. Since we are interested in obtaining the low energy neutron flux down to the thermal level, CORSIKA can not be used for this purpose. The following are tentative approaches that could be adopted in order to get the required neutron data. Analytical functions [102] can be used to get the neutron flux down to the thermal level, but they are only valid up to primaries of energy 100 GeV. GEANT4 [1] can also be used to get the neutron flux but it is limited to energies up to typical LHC level ($\sim TeV$). Therefore, it needs to be interfaced with a physical model that includes physics for higher energies and needs further investigation. Other approaches include a method [89] to calculate the lower energy neutron flux from the fast neutrons that CORSIKA provides or by using a Monte Carlo package MCNP [17].

6.2.3 Sub surface muons

Muons are capable of traveling below the surface and therefore sub-surface flux needs to be determined. In order to track muons in water [69] and underground, the MUSIC [4] (MUon SImulation Code) code can be used. It is a monte carlo code having the capability to track muons through large thickness of rock or water. This code is suited for our work because it can track muons with energies up to 10^{16} eV.

6.2.4 Experimentation

A large number of experiments are already dedicated to study the effects of cosmic rays to humans in the context of space travel. Astronauts are exposed to cosmic ray primaries, as opposed to secondary particles that we receive on the surface. As mentioned previously, such experiments are of limited importance to assess its biological damage on ground. More experiments need to be conducted on non-human samples with secondaries. There also need to be studies of mutation rate dependence on radiation on a number of biological samples to understand the phenomenon better.

Chapter 7

Discussion

The earth is most likely to have been exposed to an enhanced flux of radiation in the past. The sources of this radiation could be intense astrophysical events such as supernovae and gamma-ray bursts or radiation enhancement could occur depending on the Earth's position in the Milky Way. Such an exposure would have affected the environment and life on our planet. Good paleobiology data is available for the past $\sim$ 500 My to look for such clues in earth's history. We have developed a method to quantify the terrestrial effects of the particle component of this radiation. We have explored two major effects, (1) UVB damage from ozone depletion due to comic ray ionization in the upper stratosphere, and (2) direct impact of cosmic ray secondary muons on ground. Enhanced cosmic ray exposure can also cause climatic changes but accurate predictions are not possible due to limited knowledge of cloud microphysics.

Results are available in the form of lookup tables that can be used for other studies in the future. This method is then used to study the terrestrial effects of enhanced cosmic ray exposure from solar oscillation perpendicular to the galactic plane. This could be the possible mechanism explaining the observed periodicity in biodiversity in paleobiology databases.

Bibliography

[1] S. Agostinelli, J. Allison, K. Amako, J. Apostolakis, H. Araujo, P. Arce, M. Asai, D. Axen, S. Banerjee, G. Barrand, et al. GEANT4-a simulation toolkit. *Nuclear Instruments and Methods in Physics Research-Section A*, 506(3):250–303, 2003.

[2] E.L. Alpen. Radiation biophysics, Englewood Cliffs, NJ (US); Prentice Hall. 1990.

[3] T. Antoni, WD Apel, F. Badea, K. Bekk, A. Bercuci, H. Blumer, H. Bozdog, IM Brancus, C. Buttner, A. Chilingarian, et al. The cosmic-ray experiment KASCADE. *Nuclear Instruments and Methods in Physics Research Section A: Accelerators, Spectrometers, Detectors and Associated Equipment*, 513(3):490–510, 2003.

[4] P. Antonioli, C. Ghetti, EV Korolkova, VA Kudryavtsev, and G. Sartorelli. A three-dimensional code for muon propagation through the rock:

MUSIC. *Astroparticle Physics*, 7(4):357–368, 1997.

[5] D. Atri and A. L. Melott. Modeling high-energy cosmic ray induced terrestrial muon flux: A lookup table. *Radiation Physics and Chemistry*, in press, 2011.

[6] D. Atri, A. L. Melott, and B. C. Thomas. Lookup tables to compute high energy cosmic ray induced atmospheric ionization and changes in atmospheric chemistry. *Journal of Cosmology and Astroparticle Physics*, 5:008, May 2010.

[7] D. Atri, B. C. Thomas, and A. L. Melott. Can periodicity in low altitude cloud cover be induced by cosmic ray variability in the extragalactic shock model? *ArXiv:1006.3797, submitted*, November 2010.

[8] P.R. Band, J.J. Spinelli, VT Ng, J.A. Moody, and R.P. Gallagher. Mortality and cancer incidence in a cohort of commercial airline pilots. *Aviation, space, and environmental medicine*, 61(4):299, 1990.

[9] S. Bass. Microscopic models for ultrarelativistic heavy ion collisions. *Progress in Particle and Nuclear Physics*, 41:255–369, 1998.

[10] G. Battistoni, F. Cerutti, A. Fassò, A. Ferrari, S. Muraro, J. Ranft, S. Roesler, and P. R. Sala. The FLUKA code: description and bench-

marking. In M. Albrow & R. Raja, editor, *Hadronic Shower Simulition Workshop*, volume 896 of *American Institute of Physics Conference Series*, pages 31–49, March 2007.

[11] E. G. Berezhko and H. J. Völk. Spectrum of Cosmic Rays Produced in Supernova Remnants. *Astrophysical Journal*, 661:L175–L178, June 2007.

[12] V. Berezinsky, AZ Gazizov, and SI Grigorieva. Signatures of AGN model for UHECR. *Arxiv preprint astro-ph/0210095*, 2002.

[13] T. Bergmann, R. Engel, D. Heck, N. N. Kalmykov, S. Ostapchenko, T. Pierog, T. Thouw, and K. Werner. One-dimensional hybrid approach to extensive air shower simulation. *Astroparticle Physics*, 26:420–432, January 2007.

[14] M. Bleicher, E. Zabrodin, C. Spieles, S. A. Bass, C. Ernst, S. Soff, L. Bravina, M. Belkacem, H. Weber, H. Stöcker, and W. Greiner. Relativistic hadron-hadron collisions in the ultra-relativistic quantum molecular dynamics model. *Journal of Physics G Nuclear Physics*, 25:1859–1896, September 1999.

[15] J.D. Boice Jr, M. Blettner, and A. Auvinen. Epidemiologic studies of pilots and aircrew. *Health physics*, 79(5):576, 2000.

[16] K. Boothby, M. Chantell, KD Green, DB Kieda, J. Knapp, CG Larsen, and SP Swordy. Cosmic-Ray Composition. *The Astrophysical Journal Letters*, 491:L35–L38, 1997.

[17] J.F. Briesmeister et al. MCNP-A general Monte Carlo N-Particle transport code, version 4C. *Los Alamos National Laboratory, LA-13709-M*, 2000.

[18] J.N. Capdevielle. The karlsruhe extensive air shower simulation code corsika. *Report KfK*, 4998, 1992.

[19] J. Chen. Fluence-to-absorbed dose conversion coefficients for use in radiological protection of embryo and foetus against external exposure to protons from 100 MeV to 100 GeV. *Radiation protection dosimetry*, 118(4):378, 2006.

[20] D. B. Considine, A. R. Douglass, and C. H. Jackman. Effect of a polar stratospheric cloud parameterization on ozone depletion due to stratospheric aircraft in a two-dimensional model. *Journal of Geophysical Research*, 99:18879–18894, September 1994.

[21] J. L. Cornette and B. S. Lieberman. Random walks in the history of life. *Proceedings of the National Academy of Science*, 101:187–191, January 2004.

[22] F.A. Cucinotta and M. Durante. Cancer risk from exposure to galactic cosmic rays: implications for space exploration by human beings. *The Lancet Oncology*, 7(5):431–435, 2006.

[23] A. Dar, A. Laor, and N. J. Shaviv. Life Extinctions by Cosmic Ray Jets. *Physical Review Letters*, 80:5813–5816, June 1998.

[24] C. Dermer. GRBs as ultra-high energy cosmic ray sources: clues from Fermi. *Proceedings of "The Shocking Universe: Gamma Ray Bursts and High Energy Shock Phenomena," Venice, Italy,*, March 2010.

[25] C. D. Dermer. First Light on GRBs with Fermi. In N. Kawai & S. Nagataki, editor, *American Institute of Physics Conference Series*, volume 1279 of *American Institute of Physics Conference Series*, pages 191–199, October 2010.

[26] C. D. Dermer and J. M. Holmes. Cosmic Rays from Gamma-Ray Bursts in the Galaxy. *Astrophysical Journal Letters*, 628:L21–L24, July 2005.

[27] C.D. Dermer. Neutrino, neutron, and Cosmic-Ray production in the external shock model of gamma-ray bursts. *The Astrophysical Journal*, 574:65, 2002.

[28] T. Djemil, R. Attallah, and JN Capdevielle. Simulation of the atmospheric muon flux with CORSIKA. *International Journal of Modern Physics A*, 20(29):6950–6952, 2005.

[29] L.I. Dorman. *Cosmic rays in the earth's atmosphere and underground*. Springer Netherlands, 2004.

[30] A. R. Douglass, C. H. Jackman, and R. S. Stolarski. Comparison of model results transporting the odd nitrogen family with results transporting separate odd nitrogen species. *Journal of Geophysical Research*, 94:9862–9872, July 1989.

[31] J. Duplissy, M. B. Enghoff, K. L. Aplin, F. Arnold, H. Aufmhoff, M. Avngaard, U. Baltensperger, T. Bondo, R. Bingham, K. Carslaw, J. Curtius, A. David, B. Fastrup, S. Gagné, F. Hahn, R. G. Harrison, B. Kellett, J. Kirkby, M. Kulmala, L. Laakso, A. Laaksonen, E. Lillestol, M. Lockwood, J. Mäkelä, V. Makhmutov, N. D. Marsh, T. Nieminen, A. Onnela, E. Pedersen, J. O. P. Pedersen, J. Polny, U. Reichl, J. H. Seinfeld, M. Sipilä, Y. Stozhkov, F. Stratmann, H. Svensmark, J. Svensmark, R. Veenhof, B. Verheggen, Y. Viisanen, P. E. Wagner, G. Wehrle, E. Weingartner, H. Wex, M. Wilhelmsson, and P. M. Winkler. Results

from the CERN pilot CLOUD experiment. *Atmospheric Chemistry & Physics*, 10:1635–1647, February 2010.

[32] L. M. Ejzak, A. L. Melott, M. V. Medvedev, and B. C. Thomas. Terrestrial Consequences of Spectral and Temporal Variability in Ionizing Photon Events. *Astrophysical Journal*, 654:373–384, January 2007.

[33] J. Ellis and D. N. Schramm. Could a Nearby Supernova Explosion have Caused a Mass Extinction? *Proceedings of the National Academy of Science*, 92:235–238, January 1995.

[34] M. B. Enghoff and H. Svensmark. The role of atmospheric ions in aerosol nucleation a review. *Atmospheric Chemistry & Physics*, 8:4911–4923, August 2008.

[35] A. D. Erlykin, G. Gyalai, K. Kudela, T. Sloan, and A. W. Wolfendale. On the correlation between cosmic ray intensity and cloud cover. *Journal of Atmospheric and Solar-Terrestrial Physics*, 71:1794–1806, December 2009.

[36] A. D. Erlykin and A. W. Wolfendale. Long Term Time Variability of Cosmic Rays and Possible Relevance to the Development of Life on Earth. *Surveys in Geophysics*, 31:383–398, July 2010.

[37] A. Fasso', A. Ferrari, S. Roesler, J. Ranft, P. R. Sala, G. Battistoni, M. Campanella, F. Cerutti, L. De Biaggi, E. Gadioli, M. V. Garzelli, F. Ballarini, A. Ottolenghi, D. Scannicchio, M. Carboni, M. Pelliccioni, R. Villari, V. Andersen, A. Empl, K. Lee, L. Pinsky, T. N. Wilson, and N. Zapp. The FLUKA code: present applications and future developments. *ArXiv:0306162*, June 2003.

[38] A. Ferrari, M. Pelliccioni, and M. Pillon. Fluence-to-effective dose conversion coefficients for muons. *Radiation Protection Dosimetry*, 74(4):227, 1997.

[39] A. Ferrari, M. Pelliccioni, and T. Rancati. Calculation of the radiation environment caused by galactic cosmic rays for determining air crew exposure. *Radiation protection dosimetry*, 93(2):101, 2001.

[40] H. Fesefeldt. Report PITHA-85/02. *RWTH Aachen*, 1985.

[41] B. D. Fields, T. Athanassiadou, and S. R. Johnson. Supernova Collisions with the Heliosphere. *Astrophysical Journal*, 678:549–562, May 2008.

[42] R. S. Fletcher, T. K. Gaisser, Paolo Lipari, and Todor Stanev. sibyll: An event generator for simulation of high energy cosmic ray cascades. *Phys. Rev. D*, 50(9):5710–5731, Nov 1994.

[43] G. T. Birk, H. Lesch, and C. Konz. Solar wind induced magnetic field around the unmagnetized earth. *Astronomy and Astrophysics*, 420(2):L15–L18, 2004.

[44] T. K. Gaisser. *Cosmic Rays and Particle Physics, Cambridge, UK: Cambridge University Press*. January 1991.

[45] TK Gaisser, T. Stanev, S. Tilav, SC Corbato, HY Dai, BR Dawson, JW Elbert, B. Emerson, DB Kieda, M. Luo, et al. Cosmic-ray composition around 10^{18} eV. *Physical Review D*, 47(5):1919–1932, 1993.

[46] D. Galante and J. E. Horvath. Biological effects of gamma-ray bursts: distances for severe damage on the biota. *International Journal of Astrobiology*, 6:19–26, January 2007.

[47] N. Gehrels, C. M. Laird, C. H. Jackman, J. K. Cannizzo, B. J. Mattson, and W. Chen. Ozone Depletion from Nearby Supernovae. *Astrophysical Journal*, 585:1169–1176, March 2003.

[48] D. R. Gies and J. W. Helsel. Ice Age Epochs and the Sun's Path through the Galaxy. *Astrophysical Journal*, 626:844–848, June 2005.

[49] J.M. Grieβmeier, A. Stadelmann, U. Motschmann, NK Belisheva, H. Lammer, and HK Biernat. Cosmic ray impact on extrasolar Earth-like planets in close-in habitable zones. *Astrobiology*, 5(5):587–603, 2005.

[50] D. Groom and S. Klein. Passage of particles through matter. *The European Physical Journal C - Particles and Fields*, 15:163–173, 2000. 10.1007/BF02683419.

[51] T. Haldorsen, J.B. Reitan, and U. Tveten. Cancer incidence among Norwegian airline cabin attendants. *International journal of epidemiology*, 30(4):825, 2001.

[52] E.J. Hall, M. Astor, J. Bedford, C. Borek, S.B. Curtis, M. Fry, C. Geard, T. Hei, J. Mitchell, N. Oleinick, et al. Basic radiobiology. *American Journal of Clinical Oncology*, 11(3):220, 1988.

[53] M. B. J. Harfoot, D. J. Beerling, B. H. Lomax, and J. A. Pyle. A two-dimensional atmospheric chemistry modeling investigation of Earth's Phanerozoic O_3 and near-surface ultraviolet radiation history. *Journal of Geophysical Research (Atmospheres)*, 112:7308, April 2007.

[54] R. G. Harrison. Cloud Formation and the Possible Significance of Charge for Atmospheric Condensation and Ice Nuclei. *Space Science Reviews*, 94:381–396, November 2000.

[55] R. G. Harrison and K. S. Carslaw. Ion-aerosol-cloud processes in the lower atmosphere. *Reviews of Geophysics*, 41:1012, September 2003.

[56] T. Hebbeker and C. Timmermans. A compilation of high energy atmospheric muon data at sea level. *Astroparticle Physics*, 18:107–127, August 2002.

[57] D. Heck and J. Knapp. Extensive Air Shower Simulation with CORSIKA: A Users Guide. *Forschungszentrum Karlsruhe, Institut fur Kernphysik*, 2000.

[58] D. Heck, J. Knapp, J. N. Capdevielle, G. Schatz, and T. Thouw. *CORSIKA: a Monte Carlo code to simulate extensive air showers. 90 p., TIB Hannover, D-30167 Hannover (Germany).* February 1998.

[59] C. H. Jackman, M. T. DeLand, G. J. Labow, E. L. Fleming, D. K. Weisenstein, M. K. W. Ko, M. Sinnhuber, and J. M. Russell. Neutral atmospheric influences of the solar proton events in October-November 2003. *Journal of Geophysical Research (Space Physics)*, 110:9, July 2005.

[60] C. H. Jackman, A. R. Douglass, R. B. Rood, R. D. McPeters, and P. E. Meade. Effect of solar proton events on the middle atmosphere during the past two solar cycles as computed using a two-dimensional model. , 95:7417–7428, May 1990.

[61] C. H. Jackman, E. L. Fleming, S. Chandra, D. B. Considine, and J. E. Rosenfield. Past, present, and future modeled ozone trends with comparisons to observed trends. *Journal of Geophysical Research*, 101:28753–28768, December 1996.

[62] C. H. Jackman and R. D. McPeters. The Effect of Solar Proton Events on Ozone and Other Constituents. In J. M. Pap, P. Fox, C. Frohlich, H. S. Hudson, J. Kuhn, J. McCormack, G. North, W. Sprigg, & S. T. Wu, editor, *Solar Variability and its Effects on Climate. Geophysical Monograph 141*, volume 141 of *Washington DC American Geophysical Union Geophysical Monograph Series*, pages 305–, 2004.

[63] D. A. Juckett. Correlation of a 140-year global time signature in cancer mortality birth cohorts with galactic cosmic ray variation. *International Journal of Astrobiology*, 6:307–319, October 2007.

[64] D. A. Juckett. A 17-year oscillation in cancer mortality birth cohorts on three continents - synchrony to cosmic ray modulations one generation earlier. *International Journal of Biometeorology*, 53:487–499, June 2009.

[65] N. N. Kalmykov, G. B. Khristiansen, et al. Extensive Air Shower Data, Primary Composition and Hadron Interactions at Superhigh Energies. In *International Cosmic Ray Conference*, volume 4, page 239, 1993.

[66] P.A. Karam. Gamma and neutrino radiation dose from gamma ray bursts and nearby supernovae. *Health physics*, 82(4):491, 2002.

[67] P.A. Karam and S.A. Leslie. Calculations of background beta-gamma radiation dose through geologic time. *Health physics*, 77(6):662, 1999.

[68] Y.B. Kudryashov and M.F. Lomanov. *Radiation Biophysics (Ionizing Radiations)*. Nova Science Pub Inc, 2008.

[69] VA Kudryavtsev. Muon simulation codes MUSIC and MUSUN for underground physics. *Computer Physics Communications*, 180(3):339–346, 2009.

[70] M. Kulmala, I. Riipinen, T. Nieminen, M. Hulkkonen, L. Sogacheva, H. E. Manninen, P. Paasonen, T. Petäjä, M. Dal Maso, P. P. Aalto, A. Viljanen, I. Usoskin, R. Vainio, S. Mirme, A. Mirme, A. Minikin, A. Petzold, U. Hõrrak, C. Plaß-Dülmer, W. Birmili, and V.-M. Kerminen. Atmospheric data over a solar cycle: no connection between galactic cosmic rays and new particle formation. *Atmospheric Chemistry & Physics*, 10:1885–1898, February 2010.

[71] W. R. Leo and D. G. Haase. Techniques for Nuclear and Particle Physics Experiments. *American Journal of Physics*, 58:1216–1217, December 1990.

[72] G. Li, J. Chen, J. Ji, L. Liu, J. Yang, and X. Sheng. Global cooling forced increase in marine strontium isotopic ratios: Importance of mica weathering and a kinetic approach. *Earth and Planetary Science Letters*, 254:303–312, February 2007.

[73] M. Lockwood, R. G. Harrison, T. Woollings, and S. K. Solanki. Are cold winters in Europe associated with low solar activity? *Environmental Research Letters*, 5(2):024001, April 2010.

[74] E. Lynge. Risk of breast cancer is also increased among Danish female airline cabin attendants. *BMJ: British Medical Journal*, 312(7025):253, 1996.

[75] N. Marsh and H. Svensmark. Cosmic Rays, Clouds, and Climate. *Space Science Reviews*, 94:215–230, November 2000.

[76] N. D. Marsh and H. Svensmark . Low Cloud Properties Influenced by Cosmic Rays. *Physical Review Letters*, 85:5004–5007, December 2000.

[77] M. V. Medvedev and A. L. Melott. Do Extragalactic Cosmic Rays Induce Cycles in Fossil Diversity? *Astrophysical Journal*, 664:879–889, August 2007.

[78] A. L. Melott. Long-Term Cycles in the History of Life: Periodic Biodiversity in the Paleobiology Database. *PLoS ONE*, 3:4044, December 2008.

[79] A. L. Melott, D. Atri, B. C. Thomas, M. V. Medvedev, G. W. Wilson, and M. J. Murray. Atmospheric consequences of cosmic ray variability in the extragalactic shock model: 2. Revised ionization levels and their consequences. *Journal of Geophysical Research (Planets)*, 115:8002–, August 2010.

[80] A. L. Melott, R. K. Bambach, and K. D. Petersen. A ∼59-Myr periodic fluctuation in Strontium isotope ratios antiphase with fossil biodiversity. *arxiv:1005.4393*, February 2011.

[81] A. L. Melott and B. C. Thomas. Astrophysical Ionizing Radiation and the Earth: A Brief Review and Census of Intermittent Intense Sources. *Accepted for publication in Astrobiology, ArXiv:1102.2830*, February 2011.

[82] A.L. Melott and R.K. Bambach. A ubiquitous ∼ 62-Myr periodic fluctuation superimposed on general trends in fossil biodiversity. I. Documentation. *Paleobiology*, 37(1):92, 2011.

[83] RA Mewaldt. Cosmic rays. *Caltech article published in the Macmillan Encyclopedia of Physics*, 1996.

[84] S.R. Meyers and S.E. Peters. A 56 million year rhythm in North American sedimentation during the Phanerozoic. *Earth and Planetary Science Letters*, 2011.

[85] M. Milgrom and V. Usov. Possible association of ultra-high-energy cosmic-ray events with strong gamma-ray bursts. *The Astrophysical Journal Letters*, 449:L37, 1995.

[86] W.R. Nelson, H. Hirayama, and D.W.O. Rogers. EGS4 code system. Technical report, Stanford Linear Accelerator Center, Menlo Park, CA (USA), 1985.

[87] K. O'Brien, W. Friedberg, DF Smart, and HH Sauer. The atmospheric cosmic-and solar energetic particle radiation environment at aircraft altitudes. *Advances in Space Research*, 21(12):1739–1748, 1998.

[88] M. Pelliccioni. Overview of fluence-to-effective dose and fluence-to-ambient dose equivalent conversion coefficients for high energy radiation calculated using the FLUKA code. *Radiation Protection Dosimetry*, 88(4):279, 2000.

[89] F.M. Phillips, W.D. Stone, and J.T. Fabryka-Martin. An improved approach to calculating low-energy cosmic-ray neutron fluxes near the land/atmosphere interface. *Chemical Geology*, 175(3-4):689–701, 2001.

[90] T. Pierog, R. Engel, D. Heck, and et al. Latest Results of Air Shower Simulation Programs CORSIKA and CONEX. In *International Cosmic Ray Conference*, volume 4 of *International Cosmic Ray Conference*, pages 625–628, 2008.

[91] T. Pierog, R. Engel, D. Heck, S. Ostapchenko, and K. Werner. Latest Results from the Air Shower Simulation Programs CORSIKA and CONEX. In *Proc. 30th ICRC, Merida*, 2007.

[92] T. Pierog and K. Werner. Muon Production in Extended Air Shower Simulations. *Physical Review Letters*, 101(17):171101, October 2008.

[93] T. Pierog and K. Werner. Muon Production in Extended Air Shower Simulations. *Physical review letters*, 101(17):171101, 2008.

[94] T. Pierog and K. Werner. EPOS Model and Ultra High Energy Cosmic Rays. *Nuclear Physics B Proceedings Supplements*, 196:102–105, December 2009.

[95] H. S. Porter, C. H. Jackman, and A. E. S. Green. Efficiencies for production of atomic nitrogen and oxygen by relativistic proton impact in air. *Journal of Chemical Physics*, 65:154–167, July 1976.

[96] E. Pukkala, A. Auvinen, and G. Wahlberg. Incidence of cancer among Finnish airline cabin attendants, 1967-92. *British Medical Journal*, 311(7006):649, 1995.

[97] V. Rafnsson, J. Hrafnkelsson, and H. Tulinius. Incidence of cancer among commercial airline pilots. *Occupational and environmental medicine*, 57(3):175, 2000.

[98] J. Ranft. The Dual parton model at cosmic ray energies. *Phys. Rev.*, D51:64–84, 1995.

[99] M. V. S. Rao and B. V. Sreekantan. *Extensive air showers*. Singapore, Singapore: World Scientific, 337 p, 1998.

[100] R. A. Rohde and R. A. Muller. Cycles in fossil diversity. *Nature*, 434:208–210, March 2005.

[101] M. A. Ruderman. Possible Consequences of Nearby Supernova Explosions for Atmospheric Ozone and Terrestrial Life. *Science*, 184:1079–1081, June 1974.

[102] T. Sato and K. Niita. Analytical functions to predict cosmic-ray neutron spectra in the atmosphere. *Radiation research*, 166(3):544–555, 2006.

[103] J. Scalo and J.C. Wheeler. Astrophysical and astrobiological implications of gamma-ray burst properties. *The Astrophysical Journal*, 566:723, 2002.

[104] N. J. Shaviv. Cosmic Ray Diffusion from the Galactic Spiral Arms, Iron Meteorites, and a Possible Climatic Connection. *Physical Review Letters*, 89(5):051102, 2002.

[105] L.C. Simonsen, J.W. Wilson, M.H. Kim, and F.A. Cucinotta. Radiation exposure for human Mars exploration. *Health physics*, 79(5):515, 2000.

[106] T. Sloan and A. W. Wolfendale. Testing the proposed causal link between cosmic rays and cloud cover. *Environmental Research Letters*, 3(4):044001, April 2008.

[107] T. Stanev. *High energy cosmic rays, Chichester, UK: Springer.* 2004.

[108] T. Stanev. Ultra High Energy Cosmic Rays: origin and propagation. *Modern Physics Letters A*, 25(18):1467–1481, 2010.

[109] H. Svensmark and E. Friis-Christensen. Variation of cosmic ray flux and global cloud coverage-a missing link in solar-climate relationships. *Jour-*

nal of Atmospheric and Solar-Terrestrial Physics, 59:1225–1232, July 1997.

[110] S.P. Swordy. The energy spectra and anisotropies of cosmic rays. *Space Science Reviews*, 99:85–94, 2001. 10.1023/A:1013828611730.

[111] B. C. Thomas, C. H. Jackman, and A. L. Melott. Modeling atmospheric effects of the September 1859 solar flare. *Geophysical Research Letters*, 34:6810, March 2007.

[112] B. C. Thomas, C. H. Jackman, A. L. Melott, C. M. Laird, R. S. Stolarski, N. Gehrels, J. K. Cannizzo, and D. P. Hogan. Terrestrial Ozone Depletion due to a Milky Way Gamma-Ray Burst. *Astrophysical Journal Letters*, 622:L153–L156, April 2005.

[113] B. C. Thomas, A. L. Melott, and D. P. Hogan. Terrestrial Effects of a 30 pc Supernova. In *American Astronomical Society Meeting Abstracts*, volume 37 of *Bulletin of the American Astronomical Society*, page 1160, December 2005.

[114] B. C. Thomas, A. L. Melott, C. H. Jackman, C. M. Laird, M. V. Medvedev, R. S. Stolarski, N. Gehrels, J. K. Cannizzo, D. P. Hogan, and L. M. Ejzak. Gamma-Ray Bursts and the Earth: Exploration of

Atmospheric, Biological, Climatic, and Biogeochemical Effects. *Astrophysical Journal*, 634:509–533, November 2005.

[115] S. E. Thorsett. Terrestrial implications of cosmological gamma-ray burst models. *Astrophysical Journal*, 444:L53–L55, May 1995.

[116] B. A. Tinsley. The global atmospheric electric circuit and its effects on cloud microphysics. *Reports on Progress in Physics*, 71(6):066801, June 2008.

[117] I. G. Usoskin and G. A. Kovaltsov. Cosmic ray induced ionization in the atmosphere: Full modeling and practical applications. *Journal of Geophysical Research (Atmospheres)*, 111:21206, November 2006.

[118] I. G. Usoskin, N. Marsh, G. A. Kovaltsov, K. Mursula, and O. G. Gladysheva. Latitudinal dependence of low cloud amount on cosmic ray induced ionization. *Geophysical Research Letters*, 31:16109, August 2004.

[119] P. I. Y. Velinov and L. Mateev. Analytical approach to cosmic ray ionization by nuclei with charge Z in the middle atmosphere Distribution of galactic CR effects. *Advances in Space Research*, 42:1586–1592, November 2008.

[120] F. M. Vitt and C. H. Jackman. A comparison of sources of odd nitrogen production from 1974 through 1993 in the Earth's middle atmosphere as calculated using a two-dimensional model. *Journal of Geophysical Research*, 101:6729–6740, 1996.

[121] J. Wentz, I.M. Brancus, A. Bercuci, D. Heck, J. Oehlschlager, H. Rebel, and B. Vulpescu. Simulation of atmospheric muon and neutrino fluxes with CORSIKA. *Physical Review D*, 67(7):73020, 2003.

[122] K. Werner, Iu. Karpenko, T. Pierog, M. Bleicher, and K. Mikhailov. Event-by-event simulation of the three-dimensional hydrodynamic evolution from flux tube initial conditions in ultrarelativistic heavy ion collisions. *Phys. Rev. C*, 82(4):044904, Oct 2010.

[123] JW Wilson, SA Thibeault, FA Cucinotta, JL Shinn, M. Kim, R. Kiefer, and FF Badavi. Issues in protection from galactic cosmic rays. *Radiation and Environmental Biophysics*, 34(4):217–222, 1995.